Neurobiology of Disease

CD73 Promotes Glioblastoma Pathogenesis and Enhances Its Chemoresistance via A_{2B} Adenosine Receptor Signaling

Angela Yan,[1] Michelle L. Joachims,[3] Linda F. Thompson,[3] Andrew D. Miller,[2] Peter D. Canoll,[4] and Margaret S. Bynoe[1]

[1]Department of Microbiology and Immunology, [2]Department of Biomedical Sciences, Section of Anatomic Pathology, College of Veterinary Medicine, Cornell University, Ithaca, New York 14853, [3]Arthritis and Clinical Immunology Program, Oklahoma Medical Research Foundation, Oklahoma City, Oklahoma 73104, and [4]Department of Pathology and Cell Biology, Vagelos College of Physicians and Surgeons, Columbia University, New York City, New York 10027

Glioblastoma (GB) is one of the deadliest brain cancers to afflict humans, and it has a very poor survival rate even with treatment. The extracellular adenosine-generating enzyme CD73 is involved in many cellular functions that can be usurped by tumors, including cell adhesion, proliferation, invasion, and angiogenesis. We set out to determine the role of CD73 in GB pathogenesis. To do this, we established a unique GB mouse model (CD73-FLK) in which we spatially expressed CD73 on endothelial cells in $CD73^{-/-}$ mice. This allowed us to elucidate the mechanism of host CD73 versus GB-expressed CD73 by comparing GB pathogenesis in WT, $CD73^{-/-}$, and CD73-FLK mice. GB in $CD73^{-/-}$ mice had decreased tumor size, decreased tumor vessel density, and reduced tumor invasiveness compared with GB in WT mice. Interestingly, GBs in CD73-FLK mice were much more invasive and caused complete distortion of the brain morphology. We showed a 20-fold upregulation of A_{2B} AR on GB compared with sham, and its activation induced matrix metalloproteinase-2, which enhanced GB pathogenesis. Inhibition of A_{2B} AR signaling decreased multidrug resistance transporter protein expression, including permeability glycoprotein (P-gp) and multidrug resistance-associated protein 1 (MRP1). Further, we showed that blockade of A_{2B} AR signaling potently increased GB cell death induced by the chemotherapeutic drug temozolomide. Together, these findings suggest that CD73 and A_{2B} AR play a multifaceted role in GB pathogenesis and progression and that targeting the CD73–A_{2B} AR axis can benefit GB patients and inform new approaches for therapy to treat GB patients.

Key words: A_{2B} adenosine receptor; extracellular adenosine; CD73; glioblastoma; glioma chemoresistance; P-glycoprotein

Significance Statement

Glioblastoma (GB) is the most devastating primary brain tumor. GB patients' median survival is 16 months even with treatment. It is critical that we develop prophylaxes to advance GB treatment and improve patient survival. CD73-generated adenosine has been implicated in cancer pathogenesis, but its role in GB was not ascertained. Here, we demonstrated that host CD73 plays a prominent role in multiple areas of glioblastoma pathogenesis, including promoting GB growth, its angiogenesis, and its invasiveness. We found a 20-fold increase in A_{2B} adenosine receptor (AR) expression on GB compared with sham, and its inhibition increased GB chemosensitivity to temozolomide. These findings strongly indicate that blockade or inhibition of CD73 and the A_{2B} AR are prime targets for future GB therapy.

Introduction

Glioblastoma (GB) is the most common and most fatal primary malignant brain tumor (Wen and Kesari, 2008) due to its high capacity to proliferate and its extreme chemoresistance (Sarkaria et al., 2008). Further, the impermeability of the blood–brain barrier (BBB) makes chemotherapeutic drug delivery challenging for GB treatment (Neuwelt et al., 1982). Currently, the median survival for GB patients is 16 months even with treatment (Topkan et al., 2018).

In this report, we investigated the role of the surface enzyme CD73 (ecto-5′-nucleotidase) in GB pathogenesis as CD73 and its

Received May 2, 2018; revised March 19, 2019; accepted March 22, 2019.

Author contributions: A.Y. and M.S.B. designed research; A.Y. performed research; A.Y., A.D.M., and P.D.C. analyzed data; A.Y. wrote the first draft of the paper; A.Y., L.F.T., A.D.M., and M.S.B. edited the paper; A.Y. and M.S.B. wrote the paper; M.L.J. contributed unpublished reagents/analytic tools.

This work was supported by the National Institutes of Health (Grant RO1NS063011 to M.S.B. and RO1AI18220 to L.F.T.).

The authors declare no competing financial interests.

Correspondence should be addressed to Margaret S. Bynoe at msb76@cornell.edu.

https://doi.org/10.1523/JNEUROSCI.1118-18.2019

product, extracellular adenosine, have been implicated in the progression of other types of tumors (Zhi et al., 2007; Yegutkin et al., 2011; Zhang, 2012; Antonioli et al., 2013). CD73 is a key enzyme in the ATP metabolic pathway. In damaged tissues, ATP is released into the extracellular space (Yin et al., 2007; Cauwels et al., 2014) and converted to ADP and AMP by the surface enzyme CD39 (ectonucleoside triphosphate diphosphohydrolase-1); AMP is further converted to adenosine by CD73.

Adenosine is a purine nucleoside that promotes tumor proliferation and angiogenesis (Adair, 2005; Zhi et al., 2007). Adenosine signals through four G-protein-coupled receptors, A_1, A_{2A}, A_{2B}, and A_3, to elicit its function. The A_{2B} adenosine receptor (AR) has a very low affinity for adenosine and is activated under high, usually pathological, extracellular adenosine concentrations (in the micromolar range) (Mundell and Kelly, 1998; Haskó et al., 2009; Aherne et al., 2011; Daniele et al., 2014), whereas the A_1 AR has the highest affinity and is activated under basal adenosine concentrations (Fredholm, 2007; Müller and Jacobson, 2011). Adenosine signaling through the A_{2B} AR modulates tumor apoptosis and proliferation and the tumor immune microenvironment (Trincavelli et al., 2004; Fiebich et al., 2005; Daniele et al., 2014; Liu et al., 2014).

CD73 and adenosine are involved in tumor adhesion, invasion, proliferation, angiogenesis, and chemoresistance (Wang et al., 2003; Adair, 2005; Chan et al., 2006; Zhi et al., 2007; Bavaresco et al., 2008; Du et al., 2008; Yegutkin et al., 2011; Cappellari et al., 2012; Burnstock and Di Virgilio, 2013; Koszałka et al., 2014). For example, under hypoxic conditions, upregulation of the hypoxia inducible factor 1 (HIF-1) transcription factor increases CD73 generation of extracellular adenosine (Adair, 2005). Adenosine signaling through the A_{2A} and A_{2B} ARs induces the release of vascular endothelial growth factor (VEGF), which induces proliferation of endothelial cells and angiogenesis to promote tumor growth (Adair, 2005). CD73 and AR signaling also regulate matrix metalloproteinases (MMPs) (Chan et al., 2006; Zhi et al., 2007), which play crucial roles in angiogenesis and tumor invasion by degrading the extracellular matrix (ECM) (Zhi et al., 2007). MMP2 and MMP9 have been shown to promote GB angiogenesis and invasion and to regulate vascular patterning (Wang et al., 2003; Du et al., 2008). However, how CD73 regulates GB pathogenesis and whether host CD73 contributes to tumor pathogenesis have not been elucidated. We hypothesized that GB usurped the host and its own CD73 (GB-CD73) to promote its growth and survival. To test this, we used unique mouse models lacking CD73 or expressing CD73 on endothelial cells to study GB pathogenesis. Our data revealed that both host and GB-CD73 were key contributors to GB pathogenesis. These studies provide a potential target for GB therapeutic intervention through modulation of CD73 and/or the CD73–AR axis.

Materials and Methods

Cell culture. GL261 and U251 cell lines were obtained from National Cancer Institute and cultured in DMEM (10–013-CV, Cellgro; Corning) or RPMI 1640 (10–040-CM, Cellgro; Corning), respectively, with 10% FBS and 100 units/ml penicillin/streptomycin at 37°C/5% CO_2 in a humidified incubator. Medium was changed every 2–3 d and cells were used when grown to confluency.

Mice. C57BL/6 mice were purchased from The Jackson Laboratory. CD73$^{-/-}$ mice have been described previously (Thompson et al., 2004) and were backcrossed to C57BL/6 mice for >14 generations. Mice expressing CD73 primarily on endothelial cells (CD73-FLK mice) were produced by generating mice expressing murine CD73 under the control of the *Flk-1* promoter (see details below) and crossing them to CD73$^{-/-}$ mice. All mice used in this study were male and age matched. Mice were housed in specific-pathogen-free rooms until they were 8 weeks of age and moved to a broken barrier/biosafety level 2 room for experiments in the mouse facility at Cornell University. Animal studies were approved by the institutional animal care and use committee of Cornell University (protocol no. 2008–0092).

Generation of CD73-FLK mice. Full-length CD73 was amplified by PCR from a murine CD73 plasmid (Resta et al., 1993) to add a consensus Kozak sequence and flanking restriction sites and then cloned into a plasmid containing promoter and intronic enhancer sequences from the murine *Flk-1* gene (Kappel et al., 1999) (a gift from Dr. Lijun Xia, Oklahoma Medical Research Foundation) using NheI and EcoR I restriction sites. All plasmids were verified by sequencing. The full-length 5.4 kb transgene was released by digesting this plasmid with SalI and XmaI and, after purification, was injected into C57BL/6 blastocysts at the University of North Carolina Animal Models Core Facility. The presence of the transgene was verified by PCR using the following primers: CD73Tg forward: 5′-GGGCGGATCAAGTTCTCTGCAGC-3′; CD73Tg reverse: 5′-TTAACTGGGACTGGGGCAAAGTC-3′. Transgene-positive mice were bred to *cd73*$^{-/-}$ mice to generate offspring that expressed CD73 only under the control of the *Flk-1* promoter.

GB implantation. GL261 and GL261^{CD73low} cells were suspended in saline (15,000 cells/μl) and kept on ice. Mice were anesthetized with ketamine–xylazine (100 mg/kg) and ketoprofen (2 mg/kg) was administered as analgesic. Eye ointment was applied before hair removal. The scalps were sterilized by wiping three times with chlorhexidine solution followed by 70% ethanol. A midsagittal incision was made through the scalp and bregma was located. A small hole was drilled 0.1 mm posterior and 2.3 mm lateral of bregma. Then, 30,000 GL261 cells or saline (2 μl, sham) were injected 3 mm from the brain surface using a 27-gauge needle with a Hamilton syringe. The wound was closed using sutures and ketoprofen (2 mg/kg) was administered the day after surgery.

Tissue harvest. Mice were anesthetized with ketamine–xylazine and transcardial perfusion with ice-cold PBS was performed. Brains were cut coronally in half, flash frozen in Tissue-Tek optimal cutting temperature medium (Sakura Finetek), and stored at −80°C. Brains were sectioned to 8 or 10 μm thick with a microtome, collected on Supefrost/Plus slides (Fisher Scientific), fixed in acetone, and stored at −80°C.

Hematoxylin and eosin staining. Frozen sections were fixed with acetone, stained with 0.1% hematoxylin and 0.5% eosin, and mounted with Eukitt quick hardening mounting reagent.

Invasion score. GB invasion scores were measured using 20× scanned whole-brain images of H&E-stained brain sections taken by Aperio CS2. GB invasion scores were the sum of the meninges invasion score, the invasion area score, and the invasion distance score. The meninges invasion score equaled the ceiling of the percentage of meninges invaded divided by 5 (to transform the percentage into a score ranging from 0 to 10). The invasion area score equaled the area of tumor-infiltrating non-neoplastic area divided by the total area of the tissue section (Guillamo et al., 2009). The invasion distance score equaled the ceiling of the displacement (in micrometers) between the farthest point of the tumor infiltrating non-neoplastic area and the tumor edge (Williams et al., 2011) divided by 500 (to transform the displacement into a score ranging from 0 to 10).

Flow cytometry. GL261 and GL261^{CD73low} cells were stained with PE-conjugated antibody against mouse CD73 (1:200, 12–0731-83; eBioscience) and/or FITC-conjugated antibody against mouse CD44 (1:200, 553133; BD Biosciences), and U251 cells were stained with FITC-conjugated antibody against human CD73 (1:200, 344015; BioLegend). Cells were then washed twice with 0.5% BSA/PBS. Brain tissues were collected from GB-bearing WT mice 3 weeks after implantation. Tumors were removed with a blade and homogenized with a Dounce homogenizer in RPMI 1640 (10–040-CM, Cellgro; Corning) with 10% FBS. Tumor homogenates were centrifuged at 450 × *g* for 10 min and pellets were resuspended in 30% Percoll underlaid with 70% Percoll. Cells were centrifuged at 600 × *g* for 20 min at room temperature and the layer at the 70% and 30% Percoll junction was collected and washed with 0.5% BSA/PBS. Red blood cells were lysed with ACK lysing buffer (A1049201; Thermo Fisher Scientific) according to the manufacturer's protocol. Cells were blocked with anti-CD16/CD32 antibody (1:200, 14–0161-85;

eBioscience) and stained with PE-conjugated antibody against mouse CD73 (1:200, 12–0731-83; eBioscience). For intracellular staining, cells were fixed with 4% paraformaldehyde (15710; Electron Microscopy Sciences) for 20 min, permeabilized with 0.1% saponin (A18820; Alfa Aesar) for 15 min, and then stained with PE-conjugated antibody against mouse CD73 (1:200, eBioscience, 12–0731-83) in 0.1% saponin (Alfa Aesar, A18820). Cells were analyzed with a BD Biosciences FACSCanto II. Laser configurations were as follows: GL261 − FSC 176 V, SSC 313 V, PE 493 V, FITC 533 V; U251 − FSC 176 V, SSC 313 V, FITC 533 V; tumor homogenate − FSC 335 V, SSC 410 V, PE 400 V. Data were analyzed using FlowJo software version 10.

Immunostaining. For immunohistochemistry staining, slides were immersed in 0.3% H_2O_2 for 10 min to inactivate peroxidases. After two PBS washes, slides were blocked at room temperature with casein (Vector Laboratories) and 10% goat serum. Slides were then incubated overnight with primary antibody against CD31 (1:30; BD PharMingen, 550274), MMP9 (1:200; Millipore, AB19016), MMP2 (1:500; Millipore, MAB3308), or CD73 (1:100; BD PharMingen, 550738), followed by two PBS washes. Slides were then incubated with HRP-conjugated secondary antibody, washed, and developed with an AEC substrate kit (Zymed) and stained with hematoxylin. Slides were mounted with Fluoromount-G. For immunofluorescence staining, slides or cells grown on coverslips were blocked the same way as immunohistochemistry staining. For Ki-67 staining, slides were permeabilized using Foxp3 staining buffer set (eBioscience, 00–5523-00) following the manufacturer's protocol. Slides or coverslips were incubated overnight with primary antibody against CD73 (1:100; BD PharMingen, 550738), CD133 (1:200; Abcam, ab19898), Ki-67 (1:50; BD PharMingen, 550609), glial fibrillary acidic protein (GFAP) (1:500; BD PharMingen, 556330), NeuN (1:200; Cell Signaling Technology, 12943S), A_1 AR (1:100; Alomone Labs, AAR-006), A_{2A} AR (1:100; Alomone Labs, AAR-002), A_{2B} AR (1:100; Santa Cruz Biotechnology, SC-7507), A_3 AR (1:100; Alomone Labs, AAR-004), VEGFA (1:200; Abcam, ab46154), CD31 (1:30; BD PharMingen, 550274), α-dystroglycan (1:100; Millipore, 05–298), MMP9 (1:200; Millipore, AB19016; 1:100; Abcam, ab38898), TIMP1 (1:500; Abcam, ab86482), MMP2 (1:500; Millipore, MAB3308), P-gp (1:100; GeneTex, GTX23364), or MRP1 (1:100; Abcam, ab32574), followed by two PBS washes. Slides were then incubated with fluorophore-conjugated secondary antibody, washed, and mounted with ProLong Gold with DAPI. Slides were imaged with Zeiss Axio Imager.M1 with a Zeiss Plan-Neofluar 20× objective (44 03 40).

Sorting GL261^{CD73low} cells. GL261 cells were stained with PE-conjugated antibody against mouse CD73 (1:200; eBioscience, 12–0731-83) and washed twice with 1% FBS/PBS. Cells were sorted by a BD Biosciences FACSAria II with the following laser configurations: FSC 250 V, SSC 160 V, PE 550 V. Data were analyzed using FlowJo software version 10. Sorted cells were collected in 50% FBS in DMEM (10–013-CV, Cellgro; Corning) and cultured as normal until confluent. CD73 expression of sorted GL261^{CD73low} cells was analyzed by flow cytometry 1 d before implantation in mice.

Survival study. GB-bearing mice were monitored by their weight loss. They were killed once they lost 20% of their pre-GB implantation weight.

Isolation of primary mouse astrocytes. Primary mouse cerebellar astrocytes were isolated following Weinstein (2001). Briefly, cerebella of p4 neonatal C57BL/6 mice were ground with a Dounce homogenizer, centrifuged through 30% and 60% Percoll gradients, and astrocytes were enriched at the medium and 30% Percoll interphase. Differential adhesion was performed to enrich the astrocyte population. Primary astrocytes were cultured in DMEM (10–013-CV, Cellgro; Corning) with 10% FBS and 100 units/ml penicillin/streptomycin at 37°C/5% CO_2 in 6-well plates or on coverslips in 96-well plates in a humidified incubator until confluent. Primary astrocytes were stained with the astrocyte marker GFAP and the neuronal marker NeuN following the immunofluorescent staining protocol to verify that they were GFAP-positive and NeuN-negative.

Western blotting. Protein concentrations of GL261 and U251 whole-cell lysates and brain tissue homogenates from sham or GB-implanted mice were measured with the Dc Protein Assay (Bio-Rad); 5 μg of samples were loaded onto an 8% or 10% SDS acrylamide gel and separated for 1 h. Samples were transferred to a nitrocellulose membrane and then blocked with 1% BSA/tris-buffered saline with Tween 20 (TBST). Membrane was incubated with antibodies against A_1 AR, A_{2A} AR, A_{2B} AR, A_3 AR, P-gp, CD73, and VEGFA (1:2000; Alomone Labs, AAR-006, AAR-002, AAR-003, AAR-004; 1:1000, GeneTex, GTX108354; 1:2000, Abgent, AP2014b; 1:1000; Abcam, ab46154, respectively) overnight at 4°C. Membrane was then washed three times with TBST and incubated with HRP-conjugated secondary antibody for 1 h at room temperature. Following three TBST washes, the membrane was developed using Super Signal West Pico ECL solution (Thermo Scientific) and imaged with a Konica SRX-101A Medical Film Processor. Densitometry analysis was performed using ImageJ software. CD73 protein expression inside the GB was measured by subtracting the CD73 protein level of sham-implanted WT or CD73$^{-/-}$ coronal brain sections from CD73 protein level of GB-implanted WT or CD73$^{-/-}$ coronal brain sections.

Vessel density and glomeruloid vessel quantification. Brain sections were stained for CD31-positive vessels following the immunohistochemistry staining protocol described above. Vessel density was quantified by manually counting the number of CD31-positive vessels per area (1.5 mm^2). Glomeruloid vessels were identified by their multiple lumens in the thickened vessel wall and quantified by manually counting the number of glomeruloid vessels per area (1.5 mm^2).

qRT-PCR. Brain mRNA was extracted with TRIzol reagent (Invitrogen) and cDNA was synthesized with High-Capacity cDNA Reverse Transcription Kits (Applied Biosystems) according to the manufacturers' protocols. qRT-PCR was performed with specific primers (sequences included below) and KAPA SYBR FAST qPCR Kit (KAPA Biosystems) according to the manufacturer's protocol. qRT-PCR was done on a Bio-Rad CFX96 Real-Time System C1000 Thermal Cycler. Gene expression levels were analyzed using GAPDH as a reference gene and normalized to controls using the $2^{-\Delta\Delta CT}$ method. The following qRT-PCR primers were used: mouse MMP9 forward 5′-GCCCTGGAACTCACACGACA-3′ and reverse 5′-TTGGAAACTCACACGCCAGAAG-3′; mouse MMP2 forward 5′-AAGGATGGACTCCTGGCACATGCCTTT-3′ and reverse 5′-ACCTGTGGGCTTGTCACGT-GGTGT-3′; mouse TIMP1 forward 5′-CCAGAGCCGTCACTTTGCTT-3′ and reverse 5′-AGGAAAAGTAGACAGTGTTCAGGCTT-3′; mouse TIMP2 forward 5′-ACGCTTAGCATC-ACCCAGAAG-3′ and reverse 5′-TGGGACAGCGAGTGATCTTG-3′; human Pgp forward 5′-GCTCCTGACTATGCCAAAGC-3′ and reverse 5′-TCTTCACCTCCAGGCTCAGT-3′; mouse GAPDH forward 5′-CATGGCCTTCCGTGTTCCTA-3′ and reverse 5′-GCGGCACGTCAGAT-CCA-3′; and human GAPDH forward 5′-GGTGGTCTCCTCTGACTTCAACA-3′ and reverse 5′-GTTGCTGTAGCCAAATTCGTTGT-3′.

MMP activity measurement. MMP activity was measured according to the manufacturer's protocol using the SensoLyte 520 Generic MMP Assay Kit (AnaSpec, AS-71158). Briefly, A_{2B} AR antagonist-treated GL261 cells were collected in assay buffer and brain tissues from sham or GB-implanted mice were homogenized in assay buffer and centrifuged to remove debris. Protein concentrations were measured with the Dc Protein Assay (Bio-Rad); 400 μg of protein from each brain sample and 55.7 μg of protein from each A_{2B} AR antagonist-treated GL261 sample were incubated with MMP substrate (fluorescence resonance energy transfer peptide) for 1 h at room temperature in the dark. Fluorescence intensity was measured at Ex/Em = 490 nm/520 nm with BioTek Synergy 4. Concentrations of cleaved MMP substrate were calculated by a standard curve and normalized to sham-implanted CTs.

A_{2B} AR agonist and antagonist treatment on GB cell lines. GL261 and U251 cells were grown in 6- or 12-well plates until confluent. Culture medium was replaced with A_{2B} AR agonist (BAY 60–6583; Tocris Bioscience) or antagonist (PSB 603; Tocris Bioscience) diluted in culture medium at concentrations tested to have an optimal inhibition effect for the GL261 and U251 cells (0.1, 10, or 100 μM) or DMSO for 24 h. Cells were washed twice with PBS and then lysed with 1% Igepal CA-630 lysis buffer or with TRIzol (Invitrogen) to collect protein or mRNA for Western blotting or qRT-PCR analysis.

Rhodamine 123 (rho-123) uptake assay. GL261 cells were grown in 96-well plates or coverslips until confluent and treated with rho-123 (2.5 μM) and DMSO or PSB 603 (10–400 μM) for 4 to 24 h. Cells were then

washed with ice-cold PBS to remove extracellular rho-123. Cells in 96-well plates were lysed with 1% Igepal CA-630 lysis buffer to measure rho-123 and protein concentration with BioTek Synergy 4. Cells on coverslips were fixed and stained with anti-P-gp antibody following the immunofluorescence staining protocol.

GL261 temozolomide (TMZ) survival assay. GL261 cells grown in 12-well plates were treated with DMSO (0.54%), TMZ (30 μM), PSB 603 (100 μM), and TMZ (30 μM) + PSB 603 (100 μM) for 72 h. TMZ stock was prepared by dissolving TMZ in DMSO (20 g/ml). Both adherent cells and cells in suspension were collected and stained with 4% Trypan blue and viable/dead cell numbers were counted with a hemacytometer.

Experimental design and statistical analysis. All mice used in this study were age-matched male mice assigned randomly into sham or GB-implanted groups. All statistical analyses were performed on GraphPad Prism 6.0 software. *p*-values were calculated using one-way ANOVA followed by Bonferroni's *post hoc* test, two-way ANOVA followed by Tukey's *post hoc* test, or an unpaired 2-tailed Student's *t* test. A *p*-value of <0.05 was considered significant. Immunofluorescent intensity quantifications were performed using Zen software. Positive pixel count analyses were performed using ImageScope analysis program. Densitometry analysis for Western blot results was performed using ImageJ software.

Availability of data. The datasets used and/or analyzed during the current study are available from the corresponding author upon request. The CD73-FLK mouse is available upon request.

Results

GB cells express CD73 and upregulate their own CD73 in CD73$^{-/-}$ mice

To investigate whether GB expressed CD73, we first quantified CD73 expression *in vitro* on glioma cell lines. Both mouse GL261 and human U251 glioma cell lines expressed CD73 at 30.4% and 93.4%, respectively (Fig. 1*A*,*B*; SD = 13.45 and 13.46, respectively). Because CD44 is commonly expressed on GL261 cells, it was used as an additional marker for GL261 identification. We observed that 9.2% of GL261 cells coexpressed CD44 and CD73 (Fig. 1*C*; SD = 1.43). We then intracranially implanted mouse GL261 glioma cells or saline (sham) into C57BL/6 WT or CD73$^{-/-}$ mice to determine whether host CD73 contributed to GB pathogenesis or if CD73 expression on GB (GB-CD73) alone was sufficient to promote GB pathogenesis.

Sham-implanted and naive WT mice expressed abundant CD73 in specific brain regions, especially in the caudoputamen (Fig. 1*D*,*E*; $p < 0.0001$, $t = 20.04$, df = 16, *t* test, Fig. 1*G*,*H*; $p < 0.0001$, $t = 38.42$, df = 15, *t* test), but not in other areas such as the cortex (Fig. 1*D*,*F*; $p = 0.2544$, $t = 1.185$, df = 16, *t* test). This was compared with the absence of CD73 in sham-implanted and naive CD73$^{-/-}$ mice (Fig. 1*D*,*E*; $p < 0.0001$, $t = 20.04$, df = 16, *t* test, Fig. 1*G*,*H*; $p < 0.0001$, $t = 38.42$, df = 15, *t* test). More importantly, GB-CD73 was significantly upregulated in GB-bearing CD73$^{-/-}$ mice (Fig. 1*I*,*J*; $p = 0.0399$, $t = 2.236$, df = 16, *t* test). We also calculated GB-CD73 protein level by subtracting the GAPDH normalized CD73 level in sham WT or CD73$^{-/-}$ mice from the GAPDH normalized CD73 level in respective GB-bearing mice and compared the fold change over sham WT mice (Fig. 1*K*; $p = 0.004$, $t = 6.399$, df = 7, *t* test). We found a significant increase in GB-CD73 in CD73$^{-/-}$ mice compared with WT mice (Fig. 1*K*; $p = 0.004$, $t = 6.399$, df = 7, *t* test). To investigate whether GB-CD73 was expressed on the cell surface, we performed flow cytometry analysis on tumor cells isolated 3 weeks after GB implantation and found a similar percentage of CD73^{+} GB cells from both the permeabilized and nonpermeabilized cell populations (Fig. 1*L*; $p = 0.096$, $t = 2.168$, df = 4, *t* test). However, the median fluorescent intensity was significantly increased in permeabilized GB cells (Fig. 1*M*,*N*; $p = 0.003$, $t = 6.415$, df = 4, *t* test). This indicated that CD73 was expressed both on the cell surface and in the cytoplasm of CD73^{+} GB cells. The increased GB-CD73 expression in GB-bearing CD73$^{-/-}$ mice suggests that GB either upregulates GB-CD73 expression to compensate for the absence of host CD73, or that CD73-expressing GB cells are positively selected in the absence of host CD73. This is critical because it suggests that CD73 plays a substantial role in GB pathogenesis and that host CD73 contributes to GB pathogenesis.

Host CD73 promotes GB growth and invasiveness

To test the hypothesis that host CD73 promoted GB pathogenesis, we harvested brains from GB-bearing WT and CD73$^{-/-}$ mice and quantified GB size 17 d or 3 weeks after GB implantation. GB cells were identified by nuclear atypia, such as nuclear enlargement, pleomorphism, and hyperchromasia. The tumor border was defined as a distinct area that distinguishes between the non-neoplastic tissue and the GB tissue. GB tissue also showed distinctive tissue discoloration under H&E staining, making the tumor edge easy to identify. We found that WT mice consistently harbor significantly larger tumors compared with CD73$^{-/-}$ mice 3 weeks after implantation (Fig. 2*A*,*B*; $p = 0.0130$, $t = 2.960$, df = 11, *t* test); this was despite the increase in GB-CD73 in CD73$^{-/-}$ mice, indicating that GB-CD73 cannot fully compensate for the lack of host CD73. GB size at day 17 after implantation also showed a similar trend of reduced GB size in CD73$^{-/-}$ mice, but this was not significantly different at this time point (Fig. 2*C*,*D*; $p = 0.58$, $t = 0.59$, df = 4, *t* test). In addition to the size difference, the tumors in WT mice were more invasive 3 weeks after implantation; they penetrated the meninges and invaded other non-neoplastic areas, whereas GBs in CD73$^{-/-}$ mice remained mainly at the site of GB implantation (Fig. 2*A*). Because GBs generally do not metastasize but tend to invade surrounding tissues (characterized by tumor cells infiltrating non-neoplastic areas (Ahluwalia et al., 2010), we scored GB invasion based on meningeal invasion percentage, invasion area percentage, and distance from the invaded cells to the edge of the tumor (Guillamo et al., 2009; Williams et al., 2011). GBs in CD73$^{-/-}$ mice were significantly less invasive 3 weeks after implantation (Fig. 2*A*,*E*; $p = 0.0003$, $F_{(2,28)} = 10.77$, ANOVA), suggesting that despite increased GB-CD73, the lack of host CD73 critically hindered GB invasiveness in CD73$^{-/-}$ mice.

Vascular expression of CD73 increases GB invasiveness

To investigate how host CD73 promoted GB invasiveness in WT mice, we generated a CD73-FLK mouse model in which we enforced CD73 expression under the flk promoter (Fig. 2*F*) that was specific for endothelial cells in CD73$^{-/-}$ mice. Alexiades et al. (2015) have shown that flk is expressed on neuronal stem cells; therefore, we double stained naive CD73-FLK brain tissue with the stem cell marker CD133 and CD73. However, we did not observe CD73 expression on neuronal stem cells in CD73-FLK mice (Fig. 2*G*). We confirmed CD73 expression on the vasculature in CD73-FLK mice by immunohistochemical staining (Fig. 2*H*). CD73 was observed on vascular structures in areas such as the dentate gyrus in CD73-FLK mice, but not in WT mice (Fig. 2*H*), because WT endothelial cells do not express detectable levels of CD73 *in vivo* (Mills et al., 2008; Bynoe et al., 2015). Because GB naturally tends to invade along vascular beds (Watkins et al., 2014; Sadeghi Fazel et al., 2018) and host CD73 promotes GB invasiveness, we hypothesized that increased host CD73 along the vascular beds would further enhance GB invasiveness. Indeed, we found that GBs in CD73-FLK mice were significantly more invasive than GBs in WT mice at both 17 d and 3 weeks after implantation (Fig. 2*A*,*C*,*E*; $p = 0.0003$, $F_{(2,28)} = 10.77$, ANOVA, and I;

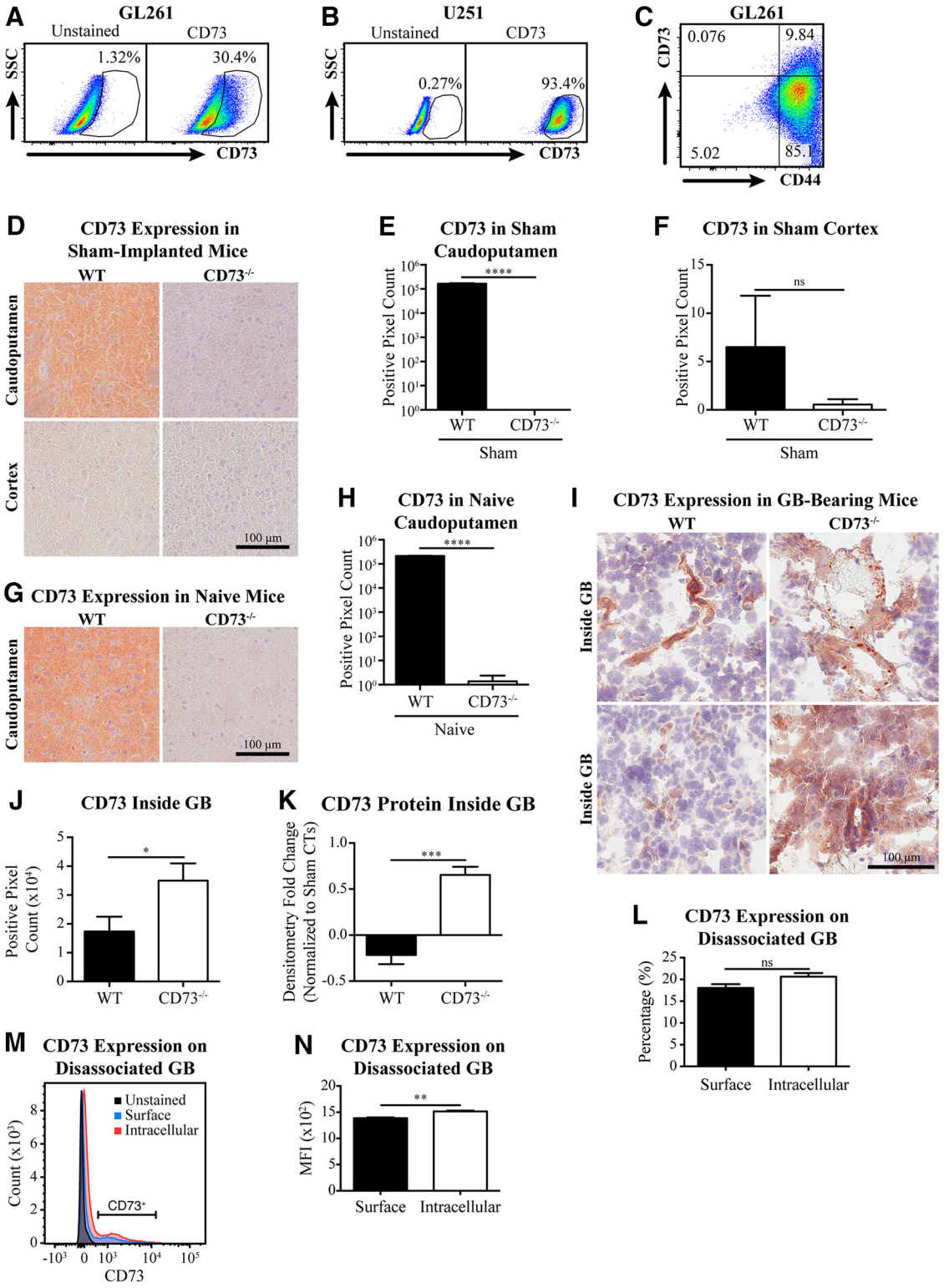

Figure 1. GB expresses CD73 *in vitro* and upregulates GB-CD73 in CD73 $^{-/-}$ mice *in vivo*. ***A***, ***B***, Representative flow cytometry analysis of CD73 expression on GL261 (***A***) and U251 (***B***) GB cell lines. Data are representative of three experiments. ***C***, Representative flow cytometry analysis of CD44 and CD73 expression on GL261. Data are representative of three experiments. ***D***, ***G***, Representative images of sham-implanted (***D***) and naive (***G***) mice brain sections stained with anti-CD73 antibody (brown) ($n = 3$). ***E***, ***F***, ***H***, Quantification of CD73 expression in caudoputamen or cortex of sham-implanted or naive mice was performed by measuring positive pixel count using ImageScope analysis program ($n = 3$, three images analyzed/sample, Student's two-tailed *t* test). ***I***, Representative images of brain sections from GL261-implanted mice stained with anti-CD73 antibody (brown) ($n = 3–4$). ***J***, Quantification of CD73 expression inside tumors was performed by measuring positive pixel count using ImageScope analysis program ($n = 3–4$, 3 images analyzed/sample, Student's two-tailed *t* test). ***K***, Densitometry quantification of CD73 protein expression inside tumors using ImageJ, normalizing to GAPDH and sham CTs ($n = 4–5$, Student's two-tailed *t* test). ***L***, ***M***, ***N***, Flow cytometry analysis of CD73 expression percentage (***L***) ($n = 3$, Student's two-tailed *t* test), histogram (***M***), and median fluorescent intensity quantification (***N***) ($n = 3$, Student's two-tailed *t* test) on disassociated tumor from GB-bearing WT mice 3 weeks after implantation ($n = 3$, Student's two-tailed *t* test). Data are shown as mean ± SEM. $^{*}p < 0.05$, $^{**}p \leq 0.01$, $^{***}p \leq 0.001$, $^{****}p < 0.0001$, ns, Nonsignificant.

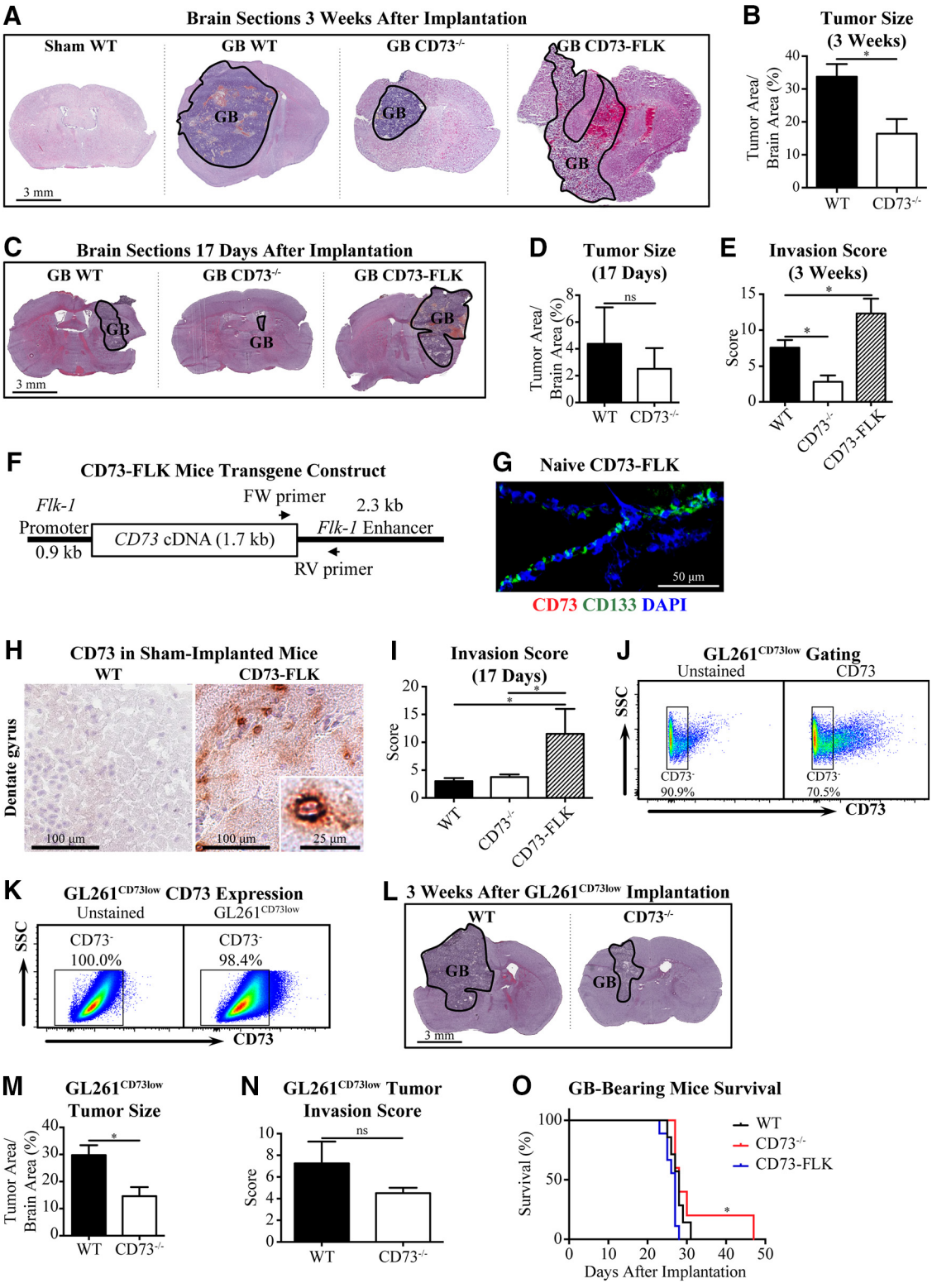

Figure 2. Host CD73 promotes GB growth and invasion. ***A***, ***C***, Representative H&E-stained brain sections from GL261- or sham-implanted mice 3 weeks after implantation (***A***) ($n = 6–7$ per group) or 17 d after implantation (***C***) ($n = 3$ per group). Solid black lines are tumor borders. ***B***, ***E***, Quantification of H&E-stained brain sections ($n = 6–7$ per group, Student's two-tailed *t* test and one-way ANOVA, respectively). ***B***, ***D***, ***M***, Tumor size is quantified by percentage of tumor area as follows: (tumor area/brain section area) × 100. ***E***, ***I***, ***N***, Tumor invasiveness was scored based on invasion area, invasion distance, and meningeal invasion. (***D***, ***I***, ***M***, ***N***) ($n = 3$ per group, Student's two-tailed *t* test for ***D***, ***M***, and ***N*** and one-way ANOVA for ***I***). ***F***, Schematic of CD73-FLK mice transgene construct. FW, Forward; RV, reverse. ***G***, Representative images of naive CD73-FLK mice brain sections stained with anti-CD73 antibody (red), CD133 (green), and DAPI (blue) ($n = 3$). ***H***, Representative images of sham-implanted WT and CD73-FLK mice brain sections stained with anti-CD73 antibody (brown) ($n = 3$). ***J***, CD73-negative gating used for sorting GL261 cells. ***K***, Flow cytometry analysis of CD73 expression on GL261 ^{CD73low} cells. ***L***, H&E-stained brain sections from GL261 ^{CD73low}-implanted mice 3 weeks after implantation ($n = 3$). Solid black lines are tumor borders. ***O***, GL261-implanted mice survival ($n = 5–9$ per group, Log-rank test). Data are shown as mean ± SEM. *$p < 0.05$, ns, Nonsignificant.

$p = 0.0288$, $F_{(2,6)} = 6.783$, ANOVA). This indicates that host CD73 expression on the vasculature significantly increases GB invasion when it is the only source of host CD73.

Host CD73 contributes more significantly to GB growth and invasiveness than GB-CD73

To investigate whether GB-CD73 contributed to GB growth and invasiveness in addition to host CD73, we sorted GL261 mouse glioma cells and selected only CD73-negative cells (referred to as GL261^{CD73low}) for implantation (Fig. 2*J*). GL261^{CD73low} cells were cultured until confluent and were implanted into WT or CD73$^{-/-}$ mice (cells were 98.4% CD73-negative at the time of implantation (Fig. 2*K*)). Three weeks after implantation, brain tissues from GB-bearing mice were analyzed by H&E staining. We found that tumors from GL261^{CD73low}-implanted CD73$^{-/-}$ mice were significantly smaller than those from GL261^{CD73low}-implanted WT mice (Fig. 2*L*,*M*; $p = 0.0379$, $t = 3.052$, df = 4, *t* test). Despite the difference in tumor size between WT and CD73$^{-/-}$ mice, the tumors were similar in size compared with their unsorted GL261-implanted counterparts (Fig. 2*B*; $p = 0.0130$, $t = 2.960$, df = 11, *t* test). This suggests that host CD73 plays a greater role in promoting GB growth than GB-CD73. Interestingly, tumors from GL261^{CD73low}-implanted WT and CD73$^{-/-}$ mice and unsorted GL261-implanted WT mice all had similar invasion scores (Fig. 2*E*; $p = 0.0003$, $F_{(2,28)} = 10.77$, ANOVA, and 2N; $p = 0.4167$, $t = 0.9050$, df = 4, *t* test). This suggests that GB-CD73 does not contribute significantly to GB invasiveness in WT mice and that, in the absence of both GB-CD73 and host CD73, other pathways regulating GB invasiveness may be induced to promote GB pathogenesis.

Absence of host CD73 prolongs the survival of GB-bearing mice

To determine whether the reduction in GB size and invasiveness in GB-bearing CD73$^{-/-}$ mice was enough to increase survival in GB-bearing mice, we implanted GL261 in WT, CD73$^{-/-}$, and CD73-FLK mice; these mice were killed after they lost 20% of their initial weight. We found that GB-bearing CD73$^{-/-}$ mice had a significant increase in survival compared with GB-bearing CD73-FLK mice (Fig. 2*O*; $p = 0.0362$, df = 2, log–rank test). This indicates that, in the absence of host CD73, GB is less pathogenic and thus prolongs survival in GB-bearing mice.

Absence of host CD73 inhibits GB angiogenesis and promotes glomeruloid vessel formation

Because GB size was significantly reduced in CD73$^{-/-}$ mice and angiogenesis is a key factor in regulating tumor growth, we next investigated whether host CD73 regulated GB angiogenesis. We found a significant decrease in vessel density within the tumors of CD73$^{-/-}$ and CD73-FLK mice (Fig. 3*A*,*B*; $p < 0.0001$, $F_{(5,37)} = 16.37$, ANOVA). Interestingly, compared with WT mice, the vessel diameter and the number of glomeruloid vessels within the tumors were increased in CD73$^{-/-}$ and CD73-FLK mice (Fig. 2*A*,*C*; $p = 0.0140$, $F_{(2,12)} = 6.228$, ANOVA, and Fig. 2*D*; $p = 0.0036$, $F_{(2,32)} = 6.740$, respectively, ANOVA). Because glomeruloid vessels are formed by highly proliferative endothelial cells (Sundberg et al., 2001), we investigated whether these GBs showed increased expression of the proliferation marker Ki-67. Indeed, Ki-67 expression was upregulated in glomeruloid vessels compared with nonglomeruloid vessels in GB (Fig. 3*E*,*F*; $p = 0.0001$, $t = 4.007$, df = 91, *t* test). In addition to nuclear Ki-67 staining, we also observed a high Ki-67 expression outside of the nucleus in glomeruloid vessels. Even though Ki-67 is mainly found in the nucleus, membrane and cytoplasmic Ki-67 expression have been found in other cancers, including breast cancer and laryngeal squamous cell carcinoma (Grzanka et al., 2000; Faratian et al., 2009). Therefore, the cytoplasmic Ki-67 expression observed in glomeruloid vessels was likely real. This increase in Ki-67 expression indicates that increased GB-CD73 in CD73$^{-/-}$ mice and increased host CD73 on the vasculature in CD73-FLK mice promote intravascular endothelial cell proliferation. However, in the absence of the full complement of host CD73 (such as in WT mice), proliferating endothelial cells cannot adequately form new vessels, suggesting that both GB-CD73 and host CD73 regulate GB angiogenesis.

Host CD73 promotes GB angiogenesis via regulating VEGF and α-dystroglycan

We next investigated whether CD73 regulated angiogenesis-related factors that contributed to the dramatic differences observed in GB vessel phenotype between GB-bearing WT and CD73$^{-/-}$ mice. We found that VEGF closely lined GB-associated blood vessels in CD73-FLK mice (Fig. 4*A*), supporting its role in GB angiogenesis. Further, we observed increased VEGF expression on GBs in CD73$^{-/-}$ mice (Fig. 4*B*,*C*; $p < 0.0001$, $F_{(3,276)} = 33.32$, ANOVA, and Fig. 4*D*; $p = 0.0084$, $F_{(3,18)} = 5.316$, ANOVA), which could lead to intravascular proliferation and increased glomeruloid vessels. This also suggests that increased GB-CD73 in GB-bearing CD73$^{-/-}$ mice promotes VEGF expression. However, the decreased vessel number indicates that host CD73 is critical for GBs to form vascular beds required for their growth and expansion.

The decrease in vessel density despite increased VEGF in GB-bearing CD73$^{-/-}$ mice was likely a result of reduced endothelial cell migration. Therefore, we next investigated the expression of α-dystroglycan, a membrane receptor that tethers the basement membranes on vessels to endothelial cells and is involved in angiogenesis regulation, endothelial cell migration, and tube formation (Gee et al., 1993; Hosokawa et al., 2002). We observed a significant increase in α-dystroglycan expression around CD31$^+$ endothelial cells inside GBs in CD73$^{-/-}$ compared with GBs in WT mice (Fig. 4*E*,*F*; $p < 0.0001$, $F_{(3,61)} = 32.05$, ANOVA). This suggests that host CD73 inhibits α-dystroglycan expression in GB and that increased α-dystroglycan and VEGF promote glomeruloid vessel formation in GB. Further, reduction in α-dystroglycan expression is also associated with poor prognosis for human GB (Zhang et al., 2014), suggesting that the absence of host CD73 lead to an improved prognosis for GB patients.

Host CD73 promotes GB angiogenesis and invasiveness through regulation of MMPs

Because both angiogenesis and invasion require remodeling of the extracellular matrix, which is often performed by MMP activities, we next investigated whether CD73 regulated MMPs and/or their inhibitors, tissue inhibitor of matrix metalloproteinases (TIMPs). We found MMP2 expression surrounding the vessels of GB, labeled by CD31 (Fig. 5*A*,*B*) and it was significantly higher in GB-implanted CD73$^{-/-}$ and CD73-FLK mice (Fig. 5*C*; $p < 0.0001$, $F_{(2,27)} = 16.87$, ANOVA). Conversely, the MMP2 inhibitor TIMP2 mRNA expression was similar in CD73$^{-/-}$, CD73-FLK, and WT GB-implanted mice (Fig. 5*D*; $p = 0.3036$, $F_{(3,22)} = 1.287$, ANOVA). This suggests that CD73 regulates MMP2 expression but not TIMP2 expression in GB and that increased GB-CD73 expression in a host with little or no CD73 promotes MMP2 upregulation.

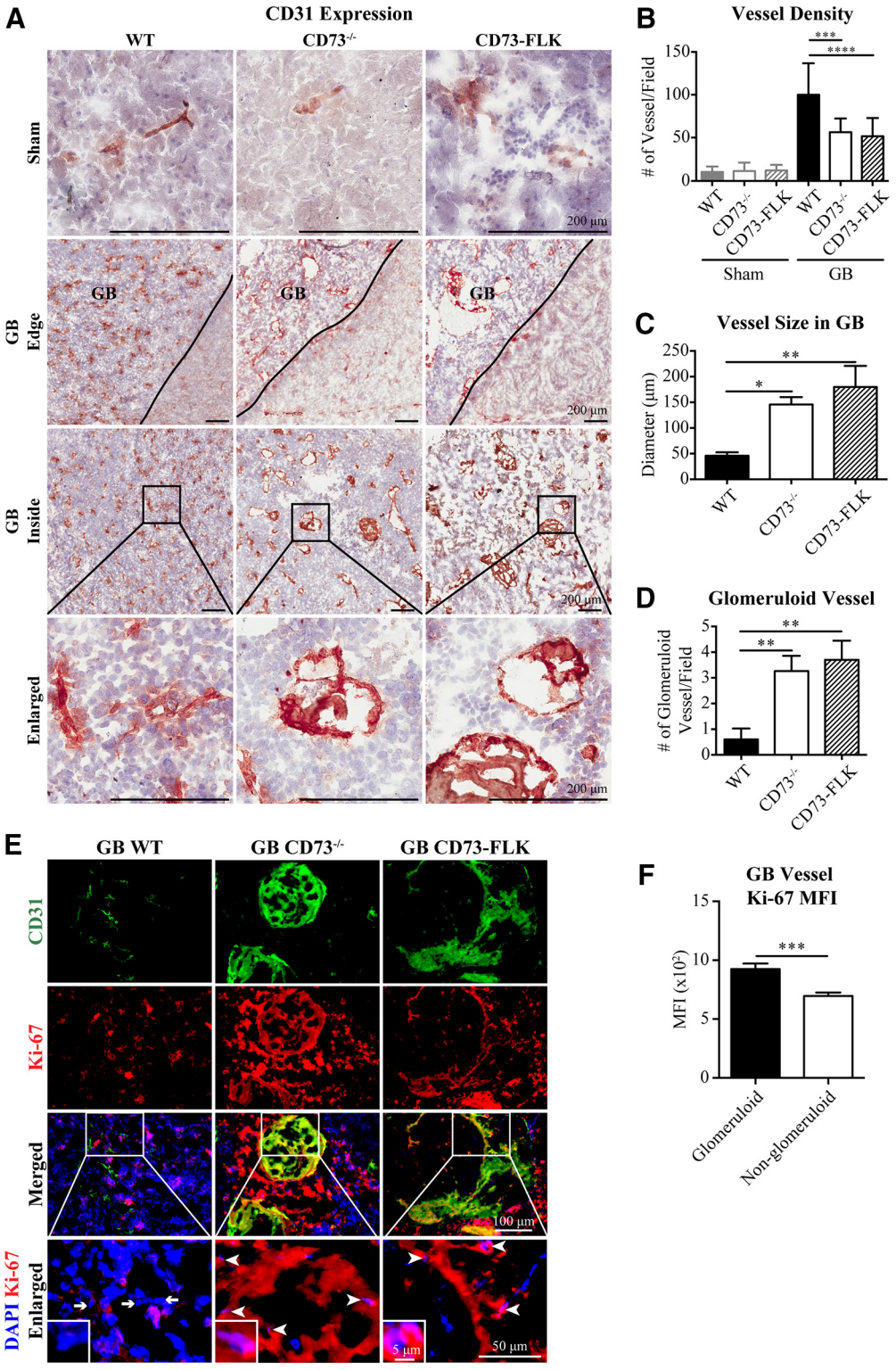

Figure 3. Absence of host CD73 inhibits GB angiogenesis and promotes glomeruloid vessel formation. ***A***, Representative images of brain sections from GL261- or sham-implanted mice stained with anti-CD31 antibody (brown) ($n = 4–6$ per GB-implanted group and $n = 2$ for sham-implanted group). ***B***, Quantification of vessel number per area (1.5 mm^2) ($n = 3–6$ per GB-implanted group and $n = 2$ per sham-implanted group, three images analyzed/sample, one-way ANOVA). ***C***, Vessel diameter measured by ImageScope software ($n = 4–6$ per group, three images analyzed/sample, one-way ANOVA). ***D***, Quantification of glomeruloid vessel number per area (1.5 mm^2) ($n = 3–5$ per group, 10 vessels analyzed/sample, one-way ANOVA). ***E***, Representative images of brain sections from GL261-implanted mice 3 weeks after implantation stained with anti-CD31 (green), anti-Ki-67 antibody (red), and DAPI (blue). Arrowheads indicate Ki-67 endothelial nuclear expression and arrows indicate the absence of Ki-67 expression in endothelial nuclei ($n = 3–4$ per group). ***F***, Ki-67 mean fluorescent intensity (MFI) quantified using Zen image analysis program ($n = 10$, 3 images analyzed/sample, 3 areas analyzed/image, Student's two-tailed *t* test). Data are shown as mean ± SEM. $*p < 0.05$, $**p \leq 0.01$, $***p \leq 0.001$, $****p < 0.0001$ (Student's two-tailed *t* test and one-way ANOVA).

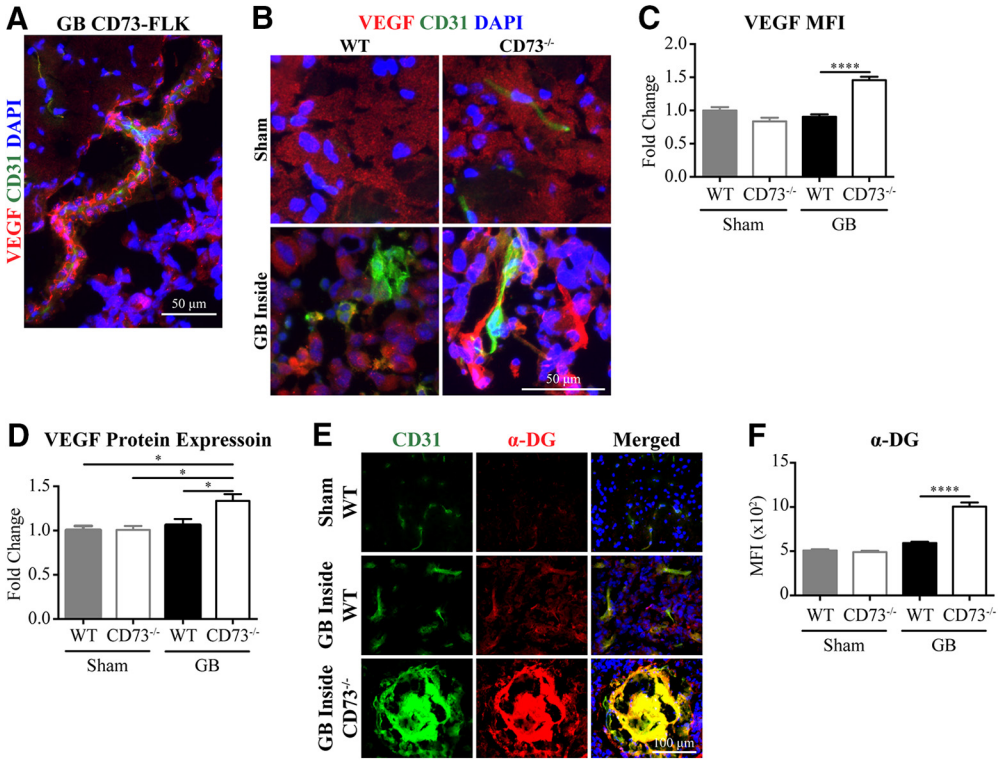

Figure 4. Host CD73 promotes GB angiogenesis via regulating VEGF and α-dystroglycan. ***A***, ***B***, Representative images of brain sections from GL261- or sham-implanted mice stained with anti-CD31 (green), anti-VEGF antibody (red), and DAPI (blue) ($n = 4–5$ per GB-implanted group and $n = 2$ per sham-implanted group). ***C***, VEGF mean fluorescent intensity (MFI) quantified using Zen image analysis program ($n = 4–5$ per GB-implanted group and $n = 2$ per sham-implanted group, 2–6 images analyzed/sample, one-way ANOVA). ***D***, Western blot densitometry analysis of VEGF ($n = 5–7$ per group, one-way ANOVA). ***E***, Representative images of brain sections from GL261- or sham-implanted mice (3 weeks after implantation) stained with anti-CD31 (green), anti-α-dystroglycan antibody (red), and DAPI (blue); images taken from inside the tumor ($n = 3–4$ per GB-implanted group and $n = 2$ per sham-implanted group). ***F***, α-dystroglycan MFI inside the tumor quantified using Zen image analysis program ($n = 3–4$ per GB-implanted group and $n = 2$ per sham-implanted group, five areas analyzed/sample, one-way ANOVA). Data are shown as mean ± SEM. $^{*}p < 0.05$, $^{****}p < 0.0001$.

We next examined MMP9 in WT and CD73$^{-/-}$ mice and found strong MMP9 expression lining the tumor's edge (Fig. 5*E–G*), which was consistent with its role in GB invasion. Interestingly, MMP9 expression at the edge of the tumor was highest in CD73-FLK mice (Fig. 5*H*; $p < 0.0001$, $F_{(2,27)} = 13.22$, ANOVA), suggesting that the increased MMP9 contributed to the increased invasiveness observed in these mice (Fig. 2*A*,*C*,*E*; $p = 0.0003$, $F_{(2,28)} = 10.77$, ANOVA, and Fig. 2*H*; $p = 0.0288$, $F_{(2,6)} = 6.783$, ANOVA) and that host CD73 expression on endothelial cells increased MMP9 expression on the edge of GBs. Even more interestingly, expression of the MMP9 inhibitor TIMP1 was significantly higher in GB-implanted CD73$^{-/-}$ mice (Fig. 5*G*,*I*; $p < 0.0001$, $F_{(2,187)} = 78.35$, ANOVA). This indicates that host CD73 inhibits TIMP1 expression and that MMP9 activity was inhibited in GB-bearing CD73$^{-/-}$ mice, leading to decreased GB invasiveness (Fig. 2*A*,*C*,*E*; $p = 0.0003$, $F_{(2,28)} = 10.77$, ANOVA, and Fig. 2*H*; $p = 0.0288$, $F_{(2,6)} = 6.783$, ANOVA). Moreover, TIMP1 expression was significantly lower in GB-bearing CD73-FLK mice compared with WT mice (Fig. 5*G*,*I*; $p < 0.0001$, $F_{(2,187)} = 78.35$, ANOVA). This suggests that host CD73 expression on endothelial cells contributes greatly to TIMP1 inhibition and results in increased GB invasiveness in CD73-FLK mice (Fig. 2*A*,*C*,*E*; $p = 0.0003$, $F_{(2,28)} = 10.77$, ANOVA, and Fig. 2*H*; $p = 0.0288$, $F_{(2,6)} = 6.783$, ANOVA). Furthermore, to determine whether MMP activity was altered in our GB models, we incubated tissue homogenates collected from sham and GB-implanted brain tissues with fluorescence resonance energy transfer (FRET) MMP substrate peptide as a MMP activity indicator. We found that MMP activity was significantly lower in homogenates from GB-bearing CD73$^{-/-}$ mice (Fig. 5*J*; $p = 0.0465$, df = 11, $t = 2.242$, t test). This indicates that, despite the increase in MMP2 expression, the overall MMP activity in GB-bearing CD73$^{-/-}$ mice is decreased compared with GB-bearing WT mice. This suggests that host CD73 regulates MMP activity in GB, including increasing MMP9 expression and inhibiting TIMP1 to promote GB invasiveness. Therefore, increased GB-CD73 alone cannot compensate for the lack of host CD73 in regulating MMP activity.

GB upregulates the A_{2B} AR *in vivo*

To elucidate whether CD73 regulates GB pathogenesis through AR signaling, we first compared AR expression on GBs with AR expression on mouse primary astrocytes from which GB cells originated. The primary astrocytes we isolated expressed the astrocyte marker GFAP, but not the neuronal marker NeuN (Fig. 6*A*). GL261 cells *in vitro* expressed A_1, A_{2A}, and A_{2B} ARs at levels similar to that of primary astrocytes, whereas A_3 AR was expressed at a much lower level (Fig. 6*B*; $p = 0.0002$, $t = 12.73$, df = 4, t test). Similarly, the human U251 GB cells expressed all four ARs (Fig. 6*C*). When we examined AR expression on sham or GB-implanted mice brain sections, A_1 and A_3 AR expression was similar between sham mice and inside GBs in both WT and CD73$^{-/-}$ mice (Fig. 6*D*,*E*,*G*; $p = 0.0043$, $F_{(3,153)} = 4.557$, ANOVA). A_{2A} AR expression was lower in GB-bearing CD73$^{-/-}$ mice, but it was not significantly different between GB and sham-implanted WT mice (Fig. 6*F*,*G*; $p = 0.0043$, $F_{(3,153)} = 4.557$, ANOVA). However, we found that the A_{2B} AR expression was

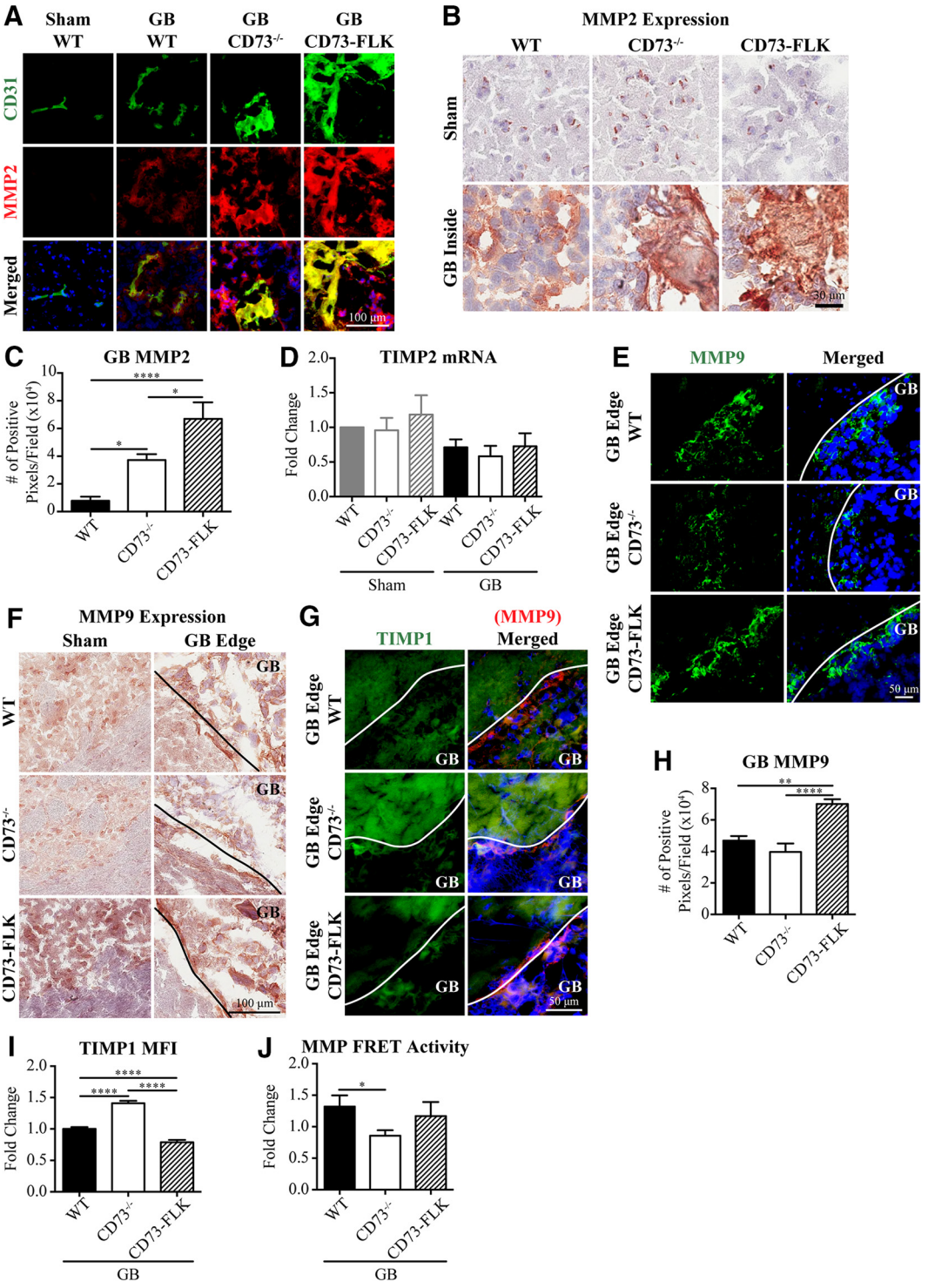

Figure 5. CD73 regulates MMP2, MMP9, and TIMP1 to promote GB invasiveness and angiogenesis. ***A***, Representative images of brain sections from GL261- or sham-implanted mice (3 weeks after implantation) stained with anti-CD31 (green), anti-MMP2 antibody (red), and DAPI (blue) ($n = 3–4$ per GB-implanted group and $n = 2$ per sham-implanted group). ***B***, Representative images of brain sections from GL261- or sham-implanted mice (3 weeks after implantation) stained with anti-MMP2 antibody (brown) ($n = 3–4$ per GB-implanted group and $n = 2$ per sham-implanted group). ***C***, MMP2 immunohistochemistry staining positive pixel count was quantified using ImageScope analysis program ($n = 3–4$ per group, three images analyzed/sample, one-way ANOVA). ***D***, qRT-PCR analysis of TIMP2 mRNA collected from GL261- or sham-implanted mice (3 weeks after implantation) ($n = 8–11$ per GB-implanted group and $n = 2–3$ per sham-implanted group, one-way ANOVA). ***E***, Representative images of brain sections from GL261- or sham-implanted mice (3 weeks after implantation) stained with anti-MMP9 antibody (green) and DAPI (blue); images taken from the edge of the tumor ($n = 3–4$ per GB-implanted group and $n = 2$ per sham-implanted group). ***F***, Representative images of brain sections from GL261- or sham-implanted mice (3 weeks after implantation) stained with anti-MMP9 antibody (brown) ($n = 3–4$ per GB-implanted group and $n = 2$ per sham-implanted group). ***G***, Representative images of brain sections from GL261- or sham-implanted mice (3 weeks after implantation) stained with anti-TIMP1 (green), anti-MMP9 antibody (red), and DAPI (blue); images taken from the edge of the tumor ($n = 4–5$ per GB-implanted group and $n = 2$ per sham-implanted group). ***H***, MMP9 immunohistochemistry staining positive pixel count on the tumor edge quantified using ImageScope analysis program ($n = 3–4$ per group, three images analyzed/sample, one-way ANOVA). ***I***, TIMP1 MFI in brain sections quantified using Zen image analysis program ($n = 4–5$, three images analyzed/sample, one-way ANOVA). ***J***, MMP activity of brain tissue homogenates from GB-bearing mice (3 weeks after implantation) normalized to sham-implanted CTs ($n = 4–7$, Student's two-tailed t test). Data are shown as mean ± SEM. $^*p < 0.05$, $^{**}p \leq 0.01$, $^{****}p < 0.0001$.

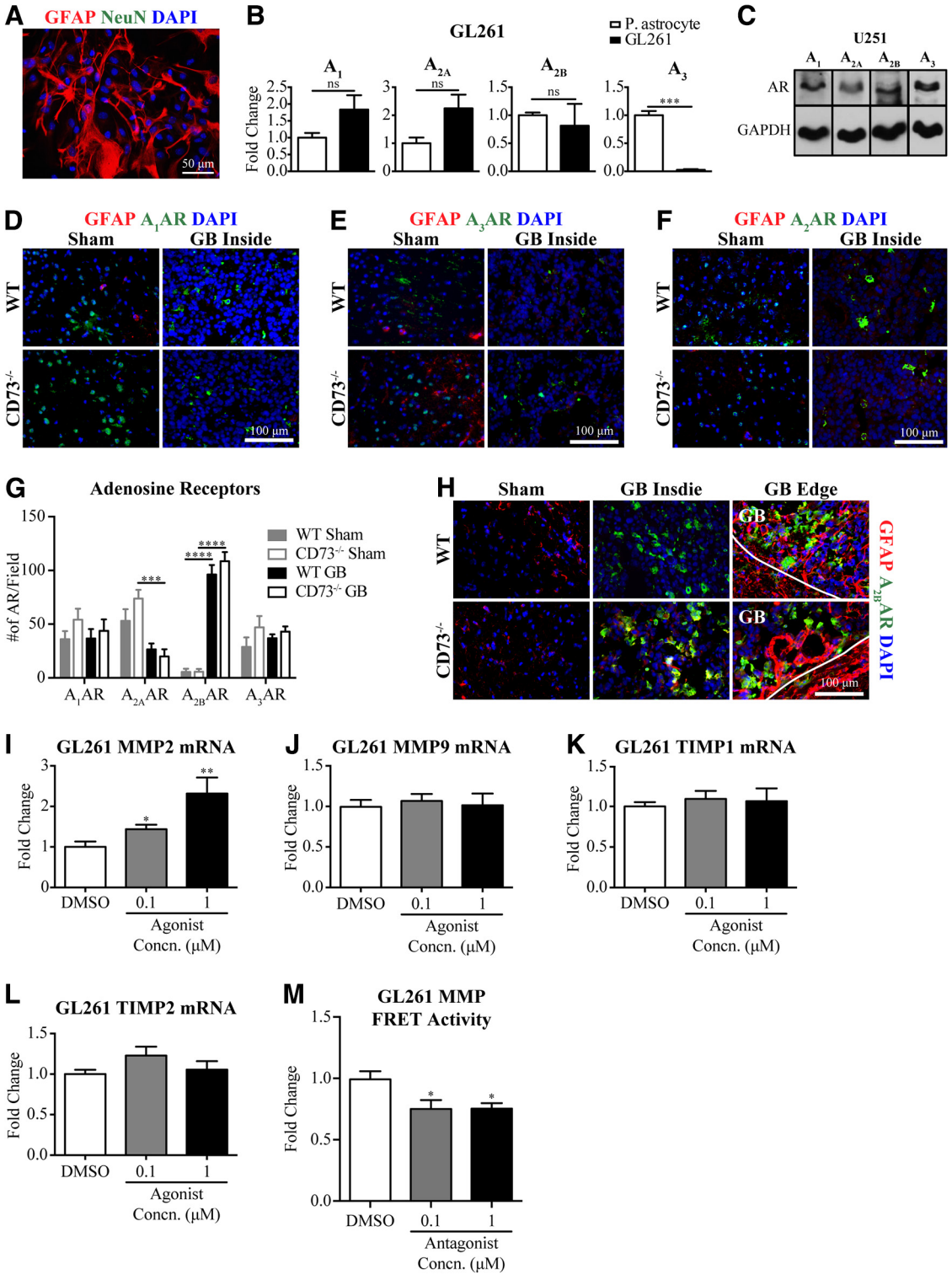

Figure 6. GB upregulates A_{2B} AR, and signaling through A_{2B} AR promotes MMP2 expression on GB. ***A***, Representative image of primary astrocyte stained with anti-GFAP antibody (red), anti-NeuN (green), and DAPI (blue). ***B***, Densitometry quantification of ARs protein expression in GL261 cells and in primary mouse astrocytes using ImageJ and normalizing to GAPDH ($n = 3$, Student's two-tailed *t* test). ***C***, Western blot analysis of ARs on human U251 cells ($n = 4$). ***D–F***, Representative images of brain sections from GL261- or sham-implanted mice (3 weeks after implantation) stained with anti-GFAP antibody (red), DAPI (blue), and anti-A_1 AR (green) (***D***), anti-A_3 AR (***E***), or anti-A_{2A} AR (***F***) ($n = 3–4$ per group). ***G***, Number of ARs per microscopic field ($n = 3–8$ per group, two-way ANOVA). ***H***, Representative images of brain sections from GL261- or sham-implanted mice (3 weeks after implantation) stained with anti-A_{2B} AR (green), anti-GFAP antibody (red), and DAPI (blue) ($n = 5–6$ per GB-implanted group and $n = 2$ per sham-treated group). ***I–L***, qRT-PCR analysis of MMP2 (***I***), MMP9 (***J***), TIMP1 (***K***), and TIMP2 (***L***) mRNA from GL261 treated with BAY 60–6583 ($n = 6$, one-way ANOVA for ***I–L***). ***M***, MMP FRET activity of GL261 cells treated with BAY 60–6583 ($n = 6$, one-way ANOVA). Data are shown as mean ± SEM. $^*p < 0.05$, $^{**}p \leq 0.01$, $^{***}p \leq 0.001$, $^{****}p < 0.0001$.

significantly upregulated by almost 20-fold in GB compared with sham *in vivo*, whereas very little expression was found on astrocytes in sham-implanted mice stained with the astrocyte marker GFAP (Fig. 6*F*; $p = 0.0043$, $F_{(3,153)} = 4.557$, ANOVA, and Fig. 6*H*). This indicates that astrocytes express very low levels of A_{2B} AR *in vivo*, whereas transformed GB cells highly upregulate A_{2B} AR *in vivo*. This is consistent with previous reports of low or diminished A_{2B} AR expression under basal conditions (Haskó et al., 2009). Because A_{2B} AR is often activated under pathological conditions (in the micromolar range) and it was highly upregulated in GBs *in vivo*, we further investigated the role that A_{2B} ARs play in GB pathogenesis.

GB A_{2B} AR signaling increases MMP2 mRNA expression and MMP activity

To investigate whether CD73 promotes GB MMP activity through A_{2B} AR signaling, we treated mouse GL261 glioma cells with the A_{2B} AR agonist BAY 60–6583 and found that activation of the A_{2B} AR upregulated MMP2 mRNA expression (Fig. 6*I*; $p = 0.0040$, $F_{(2,14)} = 8.412$, ANOVA). This suggests that the upregulation of GB-CD73 in CD73$^{-/-}$ mice (Fig. 1*J*; $p = 0.0399$, $t = 2.236$, df = 16, *t* test) increases A_{2B} AR signaling on GBs, which leads to increased MMP2 expression in GBs in CD73$^{-/-}$ mice. We found no difference in MMP9, TIMP1, and TIMP2 mRNA levels in GL261 cells upon A_{2B} AR agonist treatment (Fig. 6*J*; $p = 0.8896$, $F_{(2,15)} = 0.1178$, ANOVA, Fig. 6*K*; $p = 0.8343$, $F_{(2,15)} = 0.1834$, ANOVA, and Fig. 6*L*; $p = 0.2283$, $F_{(2,15)} = 1.633$, ANOVA). This suggests that the increased MMP9 in GB-bearing CD73-FLK mice and the increased TIMP1 in GB-bearing CD73$^{-/-}$ mice are not regulated by A_{2B} AR signaling on GB cells. Because TIMP2 expression was not altered *in vivo* in GB-bearing CD73$^{-/-}$ mice or *in vitro* through A_{2B} AR signaling on GBs, it is plausible that TIMP2 is not regulated by CD73. To determine whether changes in MMP2 mRNA expression induced by A_{2B} AR led to changes in MMP activity, we treated the mouse glioma cell line GL261 with the A_{2B} AR antagonist PSB 603 and the FRET MMP substrate peptide as a MMP activity indicator. We found that A_{2B} AR antagonist significantly decreased GL261 MMP activity (Fig. 6*M*; $p = 0.0216$, $F_{(2,15)} = 5.010$, ANOVA), suggesting that A_{2B} AR signaling on GB cells contributed to the regulation of GB-MMP activity.

A_{2B} AR signaling blockade downregulates GB multidrug resistance (MDR) transporter function and increases GB chemosensitivity

GB is resistant to most chemotherapy partly because it highly expresses MDR transporters such as P-glycoprotein (P-gp) and multidrug resistance-associated protein (MRP1) (Calatozzolo et al., 2005) (Fig. 7*A*,*B*), which expel chemotherapeutic drugs from tumor cells. We have shown that activation of A_{2A} AR increases BBB permeability by modulating P-gp function in brain endothelial cells (Carman et al., 2011; Kim and Bynoe, 2015, 2016). Because P-gp, MRP1, and A_{2B} AR were all highly upregulated in GB *in vivo* (Fig. 7*C*; $p < 0.0001$, $F_{(3,71)} = 17.15$, ANOVA, Fig. 7*D*; $p < 0.0001$, $F_{(3,77)} = 28.34$, ANOVA, Fig. 7*F*; $p = 0.0043$, $F_{(3,153)} = 4.557$, ANOVA, and Fig. 7*G*) and that MRP1 and P-gp expression were significantly higher in GB in CD73$^{-/-}$ mice (Fig. 7*C*; $p < 0.0001$, $F_{(3,71)} = 17.15$, ANOVA and Fig. 7*D*; $p < 0.0001$, $F_{(3,77)} = 28.34$, ANOVA), we hypothesized that signaling through A_{2B} AR induced the upregulation of P-gp and/or MRP1 in GB. Indeed, treatment of GL261 cells with an A_{2B} AR specific antagonist (PSB 603) dose dependently decreased both P-gp and MRP1 protein expression (Fig. 7*E*; $p = 0.0002$, $F_{(2,19)} = 14.15$, ANOVA and Fig. 7*F*; $p = 0.0123$, $F_{(2,6)} = 9.980$, ANOVA). Moreover, A_{2B} AR antagonist treatment of U251 cells also resulted in a significant decrease in P-gp mRNA expression levels (Fig. 7*G*; $p = 0.0188$, $F_{(2,5)} = 9.748$, ANOVA), indicating that A_{2B} AR signaling regulated MDR transporters both in human and mouse GB. This suggests that the increased GB-CD73 in CD73$^{-/-}$ mice (Fig. 1*J*; $p = 0.0399$, $t = 2.236$, df = 16, *t* test) results in increased activation of A_{2B} AR and thus increases P-gp and MRP1 in GB in CD73$^{-/-}$ mice (Fig. 7*C*; $p < 0.001$, $F_{(3,71)} = 17.15$, ANOVA and Fig. 7*D*; $p < 0.001$, $F_{(3,77)} = 28.34$, ANOVA).

To investigate whether inhibition of A_{2B} AR signaling leads to increased P-gp substrate uptake, we concomitantly treated GL261 cells with the P-gp substrate rho-123 and the A_{2B} AR antagonist PSB 603 and measured intracellular rho-123 uptake (Fig. 7*H*). We found that inhibition of A_{2B} AR led to increased intracellular rho-123 concentrations in the tumor cells (Fig. 7*I*,*J*; $p = 0.0277$, $t = 2.889$, df = 6, *t* test), suggesting that inhibiting A_{2B} AR signaling led to increased intracellular accumulation of P-gp substrate by downregulating P-gp expression. Because CD31^{+} endothelial cells in GBs strongly upregulated P-gp and MRP1 (Fig. 7*A*,*B*), we hypothesized that GBs regulated MDR transporters on host endothelial cells by signaling through A_{2B} AR to promote GB chemoresistance. We found that inhibition of A_{2B} AR on primary mouse brain endothelial cells also downregulated P-gp expression (Fig. 7*K*; $p = 0.0414$, $F_{(2,4)} = 7.829$, ANOVA), suggesting that increased extracellular adenosine level during pathological conditions (Haskó et al., 2009), such as in the GB microenvironment, could potentially alter host endothelial cells of the BBB through A_{2B} AR and alter BBB permeability to promote chemoresistance.

We next investigated whether A_{2B} AR antagonist treatment increased GB sensitivity to chemotherapeutic drugs by treating GL261 cells with TMZ (30 μM), a known P-gp substrate (Veringa et al., 2013), in the presence or absence of A_{2B} AR antagonist treatment for 3 d and then quantified the number of live/dead cells (Fig. 7*L*). TMZ treatment alone did not increase the percentage of dead cells but decreased the total number of cells compared with controls (Fig. 7*M*; $p < 0.0001$, $F_{(3,8)} = 279.9$, ANOVA, and Fig. 7*N*; $p < 0.0001$, $F_{(3,8)} = 65.41$, ANOVA). This indicated that GL261 cells were indeed resistant to TMZ-induced cell death and that the reduction in cell number could be a result of decreased cell proliferation. However, cotreatment with TMZ and A_{2B} AR antagonist significantly increased GL261 cell death up to 95% (Fig. 7*M*; $p < 0.0001$, $F_{(3,8)} = 279.9$, ANOVA), indicating that GB cells were more sensitive to chemotherapeutic drugs when A_{2B} AR signaling was inhibited. These findings suggest that GB uses A_{2B} AR signaling to upregulate P-gp and MRP1 expression and increase its chemoresistance. Together, these findings suggest that CD73 and the A_{2B} AR are potential targets for GB treatment.

Discussion

Purinergic molecules such as adenosine are conserved across species and play critical roles in regulating cell survival and proliferation and mediating communication between glial cells and neurons in the CNS (Fields and Burnstock, 2006). Studies have suggested that adenosine plays a significant role in cancer development and progression by attenuating the immune response (Antonioli et al., 2013). However, it was not clear how host and GB-CD73 affect GB pathogenesis and progression. In this report, we hypothesized that GBs used the purinergic enzyme CD73 to promote their growth and development. We further hypothesized that, compared with WT mice, with their full complement of host CD73, CD73$^{-/-}$ mice would produce smaller GBs. In-

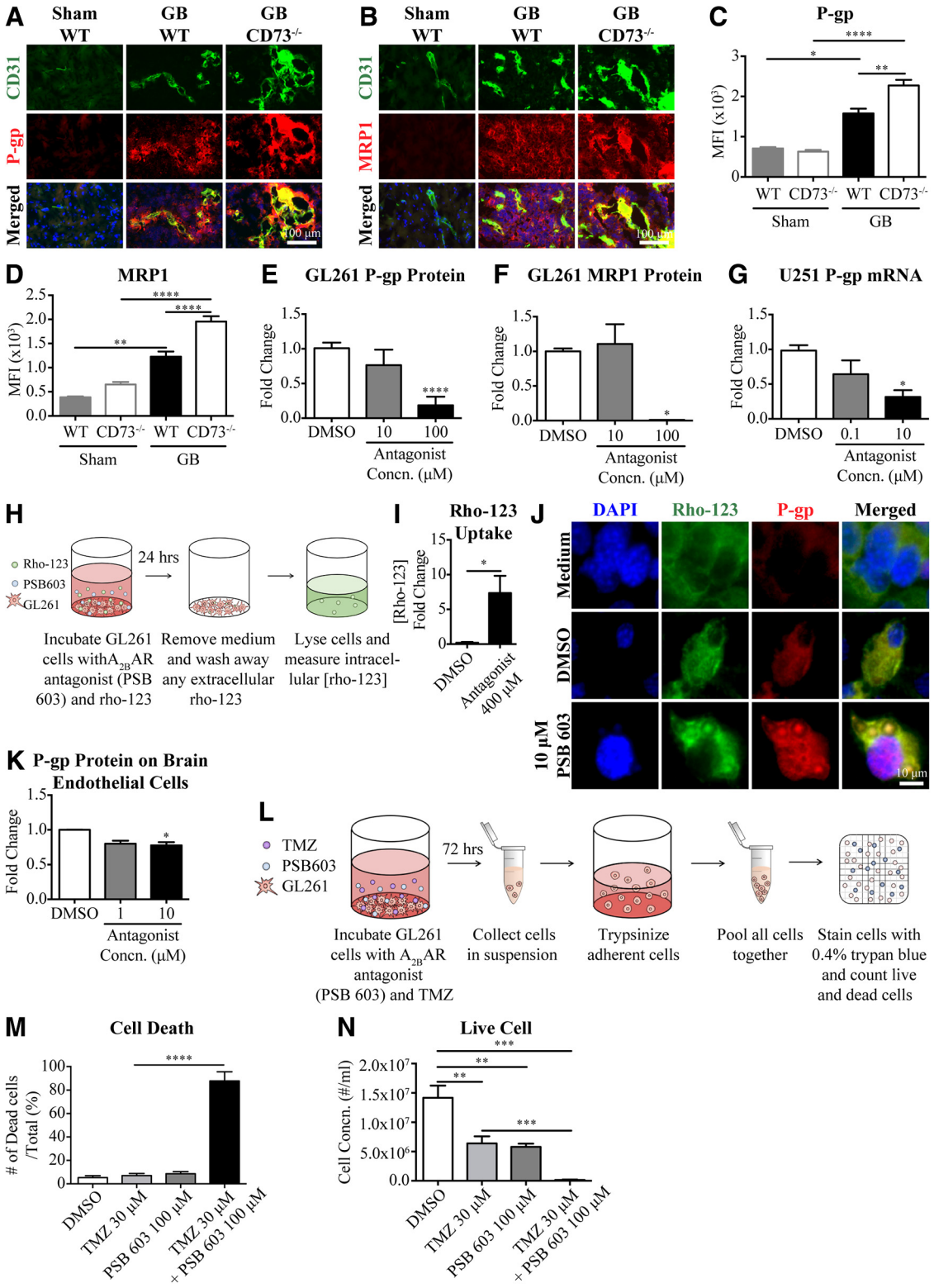

Figure 7. A_{2B} AR signaling promotes GB MDR transporter expression and enhances its chemoresistance. ***A***, ***B***, Representative images of brain sections from GL261- or sham-implanted mice (3 weeks after implantation) stained with anti-CD31 (green) and anti-P-gp antibody (red) (***A***) or anti-CD31 (green) and anti-MRP1 antibody (red) (***B***) ($n = 3–4$ per GB-implanted group and $n = 2$ per sham-implanted group). ***C***, ***D***, P-gp (***C***) and MRP1 (***D***) MFI in brain sections quantified using the Zen image analysis program ($n = 3–4$ per GB-implanted group and $n = 2$ per sham-implanted group, three images analyzed/sample, one-way ANOVA for ***C*** and ***D***). ***E***, ***F***, Western blot densitometry analysis of P-gp (***E***) ($n = 4–10$ per group) or MRP1 (***F***) ($n = 2–4$ per group, one-way ANOVA for ***E*** and ***F***) on GL261 treated with PSB 603. ***G***, qRT-PCR analysis of P-gp mRNA from U251 treated with PSB 603 ($n = 3$, one-way ANOVA). ***H***, Rho-123 uptake assay procedure. ***I***, Quantification of rho-123 concentration from GL261 cell lysate treated with PSB 603 (400 μM) relative to DMSO control ($n = 4$, Student's two-tailed t test). ***J***, GL261 treated with cell culture medium (no-treatment control), DMSO, or PSB 603 and rho-123 (green) for 4 h and stained with anti-Pgp antibody (red) and DAPI (blue) ($n = 3$). ***K***, Western blot densitometry analysis of P-gp on primary mouse brain endothelial cells treated with PSB 603 or DMSO control normalized to GAPDH using ImageJ software ($n = 2–3$ per group, one-way ANOVA). ***L***, GL261 chemotherapy sensitivity assay procedure. ***M***, ***N***, Cell death percentage (***M***) and live cell concentration (***N***) of GL261 cultured with DMSO control, TMZ (30 μM), PSB 603 (100 μM), or the latter two together for 72 h ($n = 3$, one-way ANOVA for ***M*** and ***N***). Data are shown as mean ± SEM. $^*p < 0.05$, $^{**}p \leq 0.01$, $^{***}p \leq 0.001$, $^{****}p < 0.0001$.

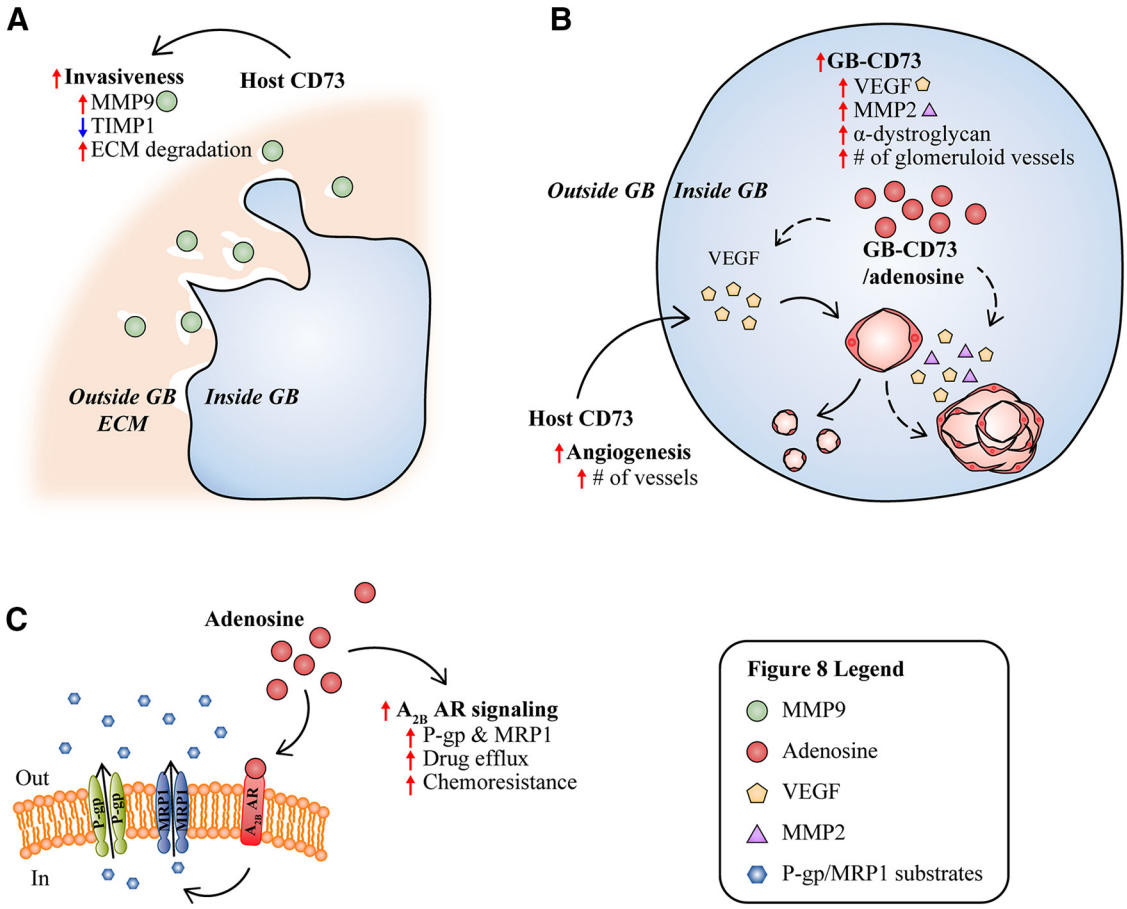

Figure 8. Working model describing how CD73 promotes GB pathogenesis. ***A***, Host CD73 promotes GB invasiveness by upregulating MMP9 and inhibiting its inhibitor, TIMP1. ***B***, Host CD73 upregulates angiogenesis by promoting mother vessels to divide into smaller vessels, thereby increasing the vessel density in GB (solid arrows). In the absence of host CD73, GB upregulates GB-CD73 and increases MMP2 expression through A_{2B} AR signaling. GB-CD73 promotes VEGF and α-dystroglycan expression, which leads to intravascular endothelial cell proliferation and glomeruloid vessel formation in GB (dotted arrows). ***C***, CD73-generated adenosine acts via the A_{2B} AR to promote P-gp and MRP1 upregulation, which results in increased drug efflux, thereby increasing GB chemoresistance.

deed, GBs in CD73$^{-/-}$ mice were significantly smaller and less invasive. Further, we showed that GBs in CD73-FLK mice were much more invasive than GBs in WT mice. This observation is in alignment with our hypothesis that host CD73 promotes GB pathogenesis, including increasing its invasiveness.

We observed that WT mice exhibited a high density of blood vessels within GBs, whereas GB-bearing CD73$^{-/-}$ mice had significantly fewer vessels. In addition, vessels in GB-bearing CD73$^{-/-}$ mice had enlarged lumens and increased glomeruloid vessel morphology. Glomeruloid vessels are surrounded by multiple layers of basement membrane and are poorly perfused (Nagy et al., 2009). The decreased vessel density causes a reduction in vessel surface area to volume ratio and is likely to result in insufficient nutrient supply. In sporadic vestibular schwannoma, vessel density is positively correlated with tumor size and growth (de Vries et al., 2012). We propose that the decreased vessel density and increased (layered) basement membrane, combined with insufficient nutrient supply, in GB-bearing CD73$^{-/-}$ mice contributed to the decreased tumor size.

We observed increased VEGF expression in GB-bearing CD73$^{-/-}$ mice. Sundberg et al. (2001) have shown that VEGF delivered by adenovirus in the ears of athymic mice is sufficient to induce and maintain glomeruloid bodies similar to GB glomeruloid vessels. This suggests that the elevated VEGF expression seen in GB-bearing CD73$^{-/-}$ mice promotes endothelial cell proliferation and glomeruloid vessel formation. However, increased α-dystroglycan in GB-bearing CD73$^{-/-}$ mice, but not in WT mice, suggests that GB endothelial cells in CD73$^{-/-}$ mice are more tightly associated with the basement membrane. Therefore, their ability to migrate and form new vessels is limited. We propose that increased VEGF, which promotes endothelial cell proliferation, along with increased α-dystroglycan expression, which reduces endothelial cell migration, lead to glomeruloid vessel formation in GBs.

In addition to VEGF and α-dystroglycan, MMP2 has been shown to regulate GB angiogenesis by promoting vascular branching (Du et al., 2008). Although we observed increased MMP2 expression in GB-bearing CD73$^{-/-}$ mice, the overall MMP activity was decreased compared with GB-bearing WT mice. This suggested that, in the absence of host CD73, MMP activity decreased, resulting in reduced vascular branching and increased glomeruloid vessel formation. This also indicates that increased GB-CD73 is insufficient to promote angiogenesis in the absence of host CD73.

The increased GB-CD73 in GB-bearing CD73$^{-/-}$ mice suggests that GB-CD73 and host CD73 have overlapping roles in GB pathogenesis. When implanted in an environment lacking CD73, CD73-positive GB cells will be selected and/or GB cells will upregulate GB-CD73 to promote their survival. To investigate whether GB-CD73 contributes to GB pathogenesis, we implanted

GL261^{CD73low} cells in WT and CD73$^{-/-}$ mice. Interestingly, GL261^{CD73low}-implanted WT and CD73$^{-/-}$ mice did not show significant alternations in GB growth. This indicates that, although host CD73 and GB-CD73 may have overlapping roles in regulating GB pathogenesis, host CD73 contributes more significantly in terms of GB growth.

The tumor microenvironment contributes significantly to tumor development, and host glial cells (astrocytes and microglia) are major producers of TIMPs, MMPs, and VEGF in the CNS (Stone et al., 1995; Pagenstecher et al., 1998; Könnecke and Bechmann, 2013; Wang et al., 2013). We investigated whether CD73 on host glial cells regulated extracellular matrix remodeling through MMPs and/or TIMPs to promote GB angiogenesis and invasion. We observed increased expression of the MMP9 inhibitor TIMP1 in GB-bearing CD73$^{-/-}$ mice. TIMP1 was observed mostly on the edge and outside the borders of GB. This suggests that TIMP1 is regulated by CD73 expressed on host cells. In addition, MMP9 expression was the highest in GB-bearing CD73-FLK mice and TIMP1 expression was the highest in GB-bearing CD73$^{-/-}$ mice, suggesting that they are both regulated by CD73. It has been shown that GB-associated microglial cells are the main contributors of MMP9 and not tumor cells (Hu et al., 2014). Therefore, because we could not find alteration in MMP9 and TIMP1 expression by antagonizing the A_{2B} AR on GB cells, it is more likely that host cells such as astrocytes and microglia are the main producers of MMP9 and TIMP1 in GB-bearing mice. Because MMP9 expression is mostly observed at the tumor edge, it is likely that it is the host cells responding to the tumor and/or the interaction between GB cells and host cells that leads to increased MMP9 at the tumor edge. This further emphasizes the importance of the host CD73 in GB pathogenesis.

Additionally, because CD73 is a prominent immune regulator, the host immune response against GB may be significantly altered in CD73$^{-/-}$ mice. For instance, CD73$^{-/-}$ microglial cells do not become ramified when exposed to ATP (Matyash et al., 2017) and this can significantly alter GB pathogenesis. Therefore, the upregulation of GB-CD73 in CD73$^{-/-}$ mice was unable to fully compensate for the lack of host CD73 in the host environment.

We found increased GB P-gp and MRP1 expression in CD73$^{-/-}$ mice. GB cells were also more sensitive to chemotherapeutic drugs when GB A_{2B} AR signaling was inhibited. We showed that A_{2B} AR signaling in GB promotes GB chemoresistance by upregulating P-gp and MRP1. These data suggest that GB-CD73 is the main driver of GB MDR transporter expression and show that both host CD73 and GB-CD73 contribute to GB pathogenesis independently. As a result, when using anti-CD73 antibody or CD73 inhibitor as a treatment, it is important to know that host and GB may respond to the treatment differently and that targeting specific cells may help to predict the treatment outcome.

We showed that A_{2B} AR played a critical role in GB pathogenesis. Because A_{2B} AR has a low affinity for adenosine compared with other adenosine receptors, this further supports the hypothesis that A_{2B} AR is activated during high/pathological adenosine concentrations (Mundell and Kelly, 1998; Haskó et al., 2009; Aherne et al., 2011; Daniele et al., 2014) such as during hypoxia and inflammation. This coincides with our findings of increased A_{2B} AR in pathological GB conditions compared with sham mice and its involvement in regulating MMP activity and MDR transporters in GB.

Based on these findings, we propose that GB uses host CD73 to increase MMP9 expression and inhibit TIMP1 to promote GB invasion (Fig. 8*A*). Host CD73 also promotes GB angiogenesis by increasing GB vessel number (Fig. 8*B*). The absence of host CD73 leads to increased GB-CD73, VEGF, MMP2, and α-dystroglycan and results in the formation of glomeruloid vessels (Fig. 8*B*). Finally, A_{2B} AR signaling on GB cells promotes P-gp/MRP1 expression and increases GB chemoresistance (Fig. 8*C*).

GB is the deadliest of all brain tumors, with a median patient survival up to 16 months, even with treatment (Topkan et al., 2018). Here, we demonstrated multiple pathways of host and GB-CD73 contribution to GB pathogenesis, such as GB angiogenesis, invasion, and its chemoresistance. These studies indicate that by modulating host CD73, GB-CD73/AR_{2B} AR signaling may significantly improve treatment and increase the lifespan of GB patients.

References

Adair TH (2005) Growth regulation of the vascular system: an emerging role for adenosine. Am J Physiol Regul Integr Comp Physiol 289:R283–R296.

Aherne CM, Kewley EM, Eltzschig HK (2011) The resurgence of A2B adenosine receptor signaling. Biochim Biophys Acta 1808:1329–1339.

Ahluwalia MS, de Groot J, Liu WM, Gladson CL (2010) Targeting SRC in glioblastoma tumors and brain metastases: rationale and preclinical studies. Cancer Lett 298:139–149.

Alexiades NG, Auffinger B, Kim CK, Hasan T, Lee G, Deheeger M, Tobias AL, Kim J, Balyasnikova I, Lesniak MS, Aboody K, Ahmed AU (2015) MMP14 as a novel downstream target of VEGFR2 in migratory gliomatropic neural stem cells. Stem Cell Res 15:598–607.

Antonioli L, Blandizzi C, Pacher P, Haskó G (2013) Immunity, inflammation and cancer: a leading role for adenosine. Nat Rev Cancer 13:842–857.

Bavaresco L, Bernardi A, Braganhol E, Cappellari AR, Rockenbach L, Farias PF, Wink MR, Delgado-Cañedo A, Battastini AM (2008) The role of ecto-5′nucleotidase/CD73 in glioma cell line proliferation. Mol Cell Biochem 319:61–68.

Burnstock G, Di Virgilio F (2013) Purinergic signalling and cancer. Purinergic Signal 9:491–540.

Bynoe MS, Viret C, Yan A, Kim DG (2015) Adenosine receptor signaling: a key to opening the blood-brain door. Fluids Barriers CNS 12:20.

Calatozzolo C, Gelati M, Ciusani E, Sciacca FL, Pollo B, Cajola L, Marras C, Silvani A, Vitellaro-Zuccarello L, Croci D, Boiardi A, Salmaggi A (2005) Expression of drug resistance proteins pgp, MRP1, MRP3, MRP5 and GST-π in human glioma. J Neurooncol 74:113–121.

Cappellari AR, Vasques GJ, Bavaresco L, Braganhol E, Battastini AM (2012) Involvement of ecto-5′-nucleotidase/CD73 in U138MG glioma cell adhesion. Mol Cell Biochem 359:315–322.

Carman AJ, Mills JH, Krenz A, Kim DG, Bynoe MS (2011) Adenosine receptor signaling modulates permeability of the blood-brain barrier. J Neurosci 31:13272–13280.

Cauwels A, Rogge E, Vandendriessche B, Shiva S, Brouckaert P (2014) Extracellular ATP drives systemic inflammation, tissue damage and mortality. Cell Death Dis 5:e1102.

Chan ES, Montesinos MC, Fernandez P, Desai A, Delano DL, Yee H, Reiss AB, Pillinger MH, Chen JF, Schwarzschild MA, Friedman SL, Cronstein BN (2006) Adenosine A(2A) receptors play a role in the pathogenesis of hepatic cirrhosis. Br J Pharmacol 148:1144–1155.

Daniele S, Zappelli E, Natali L, Martini C, Trincavelli ML (2014) Modulation of A1 and A2B adenosine receptor activity: a new strategy to sensitise glioblastoma stem cells to chemotherapy. Cell Death Dis 5:e1539.

de Vries M, Hogendoorn PC, Briaire-de Bruyn I, Malessy MJ, van der Mey AG (2012) Intratumoral hemorrhage, vessel density, and the inflammatory reaction contribute to volume increase of sporadic vestibular schwannomas. Virchows Arch 460:629–636.

Du R, Petritsch C, Lu K, Liu P, Haller A, Ganss R, Song H, Vandenberg S, Bergers G (2008) Matrix metalloproteinase-2 regulates vascular patterning and growth affecting tumor cell survival and invasion in GBM. Neuro Oncol 10:254–264.

Faratian D, Munro A, Twelves C, Bartlett JM (2009) Membranous and cytoplasmic staining of Ki67 is associated with HER2 and ER status in invasive breast carcinoma. Histopathology 54:254–257.

Fiebich BL, Akundi RS, Biber K, Hamke M, Schmidt C, Butcher RD, van

Calker D, Willmroth F (2005) IL-6 expression induced by adenosine A2b receptor stimulation in U373 MG cells depends on p38 mitogen activated kinase and protein kinase C. Neurochem Int 46:501–512.
Fields RD, Burnstock G (2006) Purinergic signalling in neuron-glia interactions. Nat Rev Neurosci 7:423–436.
Fredholm BB (2007) Adenosine, an endogenous distress signal, modulates tissue damage and repair. Cell Death Differ 14:1315–1323.
Gee SH, Blacher RW, Douville PJ, Provost PR, Yurchenco PD, Carbonetto S (1993) Laminin-binding protein 120 from brain is closely related to the dystrophin-associated glycoprotein, dystroglycan, and binds with high affinity to the major heparin binding domain of laminin. J Biol Chem 268:14972–14980.
Grzanka A, Sujkowska R, Janiak A, Adamska M (2000) Immunogold labelling of PCNA and Ki-67 antigen at the ultrastructural level in laryngeal squamous cell carcinoma and its correlation with lymph node metastasis and histological grade. Acta Histochem 102:139–149.
Guillamo JS, de Boüard S, Valable S, Marteau L, Leuraud P, Marie Y, Poupon MF, Parienti JJ, Raymond E, Peschanski M (2009) Molecular mechanisms underlying effects of epidermal growth factor receptor inhibition on invasion, proliferation, and angiogenesis in experimental glioma. Clin Cancer Res 15:3697–3704.
Haskó G, Csóka B, Németh ZH, Vizi ES, Pacher P (2009) A2B adenosine receptors in immunity and inflammation. Trends Immunol 30:263–270.
Hosokawa H, Ninomiya H, Kitamura Y, Fujiwara K, Masaki T (2002) Vascular endothelial cells that express dystroglycan are involved in angiogenesis. J Cell Sci 115:1487–1496.
Hu F, Ku MC, Markovic D, Dzaye O, Lehnardt S, Synowitz M, Wolf SA, Kettenmann H (2014) Glioma associated microglial MMP9 expression is up regulated by TLR2 signalling and sensitive to minocycline. Int J Cancer 135:2569–2578.
Kappel A, Rönicke V, Damert A, Flamme I, Risau W, Breier G (1999) Identification of vascular endothelial growth factor (VEGF) receptor-2 (Flk-1) promoter/enhancer sequences sufficient for angioblast and endothelial cell-specific transcription in transgenic mice. Blood 93:4284–4292.
Kim DG, Bynoe MS (2015) A2A adenosine receptor regulates the human blood-brain barrier permeability. Mol Neurobiol 52:664–678.
Kim DG, Bynoe MS (2016) A2A adenosine receptor modulates drug efflux transporter P-glycoprotein at the blood-brain barrier. J Clin Invest 126:1717–1733.
Könnecke H, Bechmann I (2013) The role of microglia and matrix metalloproteinases involvement in neuroinflammation and gliomas. Clin Dev Immunol 2013:914104.
Koszałka P, Pryszlak A, Gołuńska M, Kolasa J, Stasiłojć G, Składanowski AC, Bigda JJ (2014) Inhibition of CD73 stimulates the migration and invasion of B16F10 melanoma cells in vitro, but results in impaired angiogenesis and reduced melanoma growth in vivo. Oncol Rep 31:819–827.
Liu TZ, Wang X, Bai YF, Liao HZ, Qiu SC, Yang YQ, Yan XH, Chen J, Guo HB, Zhang SZ (2014) The HIF-2alpha dependent induction of PAP and adenosine synthesis regulates glioblastoma stem cell function through the A2B adenosine receptor. Int J Biochem Cell Biol 49:8–16.
Matyash M, Zabiegalov O, Wendt S, Matyash V, Kettenmann H (2017) The adenosine generating enzymes CD39/CD73 control microglial processes ramification in the mouse brain. PLoS One 12:e0175012.
Mills JH, Thompson LF, Mueller C, Waickman AT, Jalkanen S, Niemela J, Airas L, Bynoe MS (2008) CD73 is required for efficient entry of lymphocytes into the central nervous system during experimental autoimmune encephalomyelitis. Proc Natl Acad Sci U S A 105:9325–9330.
Müller CE, Jacobson KA (2011) Recent developments in adenosine receptor ligands and their potential as novel drugs. Biochim Biophys Acta 1808:1290–1308.
Mundell SJ, Kelly E (1998) Evidence for co-expression and desensitization of A2a and A2b adenosine receptors in NGl08–15 cells. Biochem Pharmacol 55:595–603.
Nagy JA, Chang SH, Dvorak AM, Dvorak HF (2009) Why are tumour blood vessels abnormal and why is it important to know? Br J Cancer 100: 865–869.
Neuwelt EA, Barnett PA, Bigner DD, Frenkel EP (1982) Effects of adrenal cortical steroids and osmotic blood-brain barrier opening on methotrexate delivery to gliomas in the rodent: the factor of the blood-brain barrier. Proc Natl Acad Sci U S A 79:4420–4423.
Pagenstecher A, Stalder AK, Kincaid CL, Shapiro SD, Campbell IL (1998) Differential expression of matrix metalloproteinase and tissue inhibitor of matrix metalloproteinase genes in the mouse central nervous system in normal and inflammatory states. Am J Pathol 152:729–741.
Resta R, Hooker SW, Hansen KR, Laurent AB, Park JL, Blackburn MR, Knudsen TB, Thompson LF (1993) Murine ecto-5′-nucleotidase (CD73): cDNA cloning and tissue distribution. Gene 133:171–177.
Sadeghi Fazel FS, Derakhshanrad N, Yekaninejad MS, Vosoughi F, Derakhshanrad A, Saberi H (2018) Predictive value of braden risk factors in pressure ulcers of outpatients with spinal cord injury. Acta Med Iran 56:56–61.
Sarkaria JN, Kitange GJ, James CD, Plummer R, Calvert H, Weller M, Wick W (2008) Mechanisms of chemoresistance to alkylating agents in malignant glioma. Clin Cancer Res 14:2900–2908.
Stone J, Itin A, Alon T, Pe'er J, Gnessin H, Chan-Ling T, Keshet E (1995) Development of retinal vasculature is mediated by hypoxia-induced vascular endothelial growth factor (VEGF) expression by neuroglia. J Neurosci 15:4738–4747.
Sundberg C, Nagy JA, Brown LF, Feng D, Eckelhoefer IA, Manseau EJ, Dvorak AM, Dvorak HF (2001) Glomeruloid microvascular proliferation follows adenoviral vascular permeability Factor/Vascular endothelial growth factor-164 gene delivery. Am J Pathol 158:1145–1160.
Thompson LF, Eltzschig HK, Ibla JC, Van De Wiele CJ, Resta R, Morote-Garcia JC, Colgan SP (2004) Crucial role for ecto-5′-nucleotidase (CD73) in vascular leakage during hypoxia. J Exp Med 200:1395–1405.
Topkan E, Selek U, Ozdemir Y, Yildirim BA, Guler OC, Ciner F, Mertsoylu H, Tufan K (2018) Prognostic value of the Glasgow prognostic score for glioblastoma multiforme patients treated with radiotherapy and temozolomide. J Neurooncol 139:411–419.
Trincavelli ML, Marroni M, Tuscano D, Ceruti S, Mazzola A, Mitro N, Abbracchio MP, Martini C (2004) Regulation of A2B adenosine receptor functioning by tumour necrosis factor a in human astroglial cells. J Neurochem 91:1180–1190.
Veringa SJ, Biesmans D, van Vuurden DG, Jansen MH, Wedekind LE, Horsman I, Wesseling P, Vandertop WP, Noske DP, Kaspers GJ, Hulleman E (2013) In vitro drug response and efflux transporters associated with drug resistance in pediatric high grade glioma and diffuse intrinsic pontine glioma. PLoS One 8:e61512.
Wang L, Cossette SM, Rarick KR, Gershan J, Dwinell MB, Harder DR, Ramchandran R (2013) Astrocytes directly influence tumor cell invasion and metastasis in vivo. PLoS One 8:e80933.
Wang M, Wang T, Liu S, Yoshida D, Teramoto A (2003) The expression of matrix metalloproteinase-2 and-9 in human gliomas of different pathological grades. Brain Tumor Pathol 20:65–72.
Watkins S, Robel S, Kimbrough IF, Robert SM, Ellis-Davies G, Sontheimer H (2014) Disruption of astrocyte-vascular coupling and the blood-brain barrier by invading glioma cells. Nat Commun 5:4196.
Weinstein DE (2001) Isolation and purification of primary rodent astrocytes. Curr Protoc Neurosci Chapter 3:Unit 3.5.
Wen PY, Kesari S (2008) Malignant gliomas in adults. N Engl J Med 359: 492–507.
Williams SP, Nowicki MO, Liu F, Press R, Godlewski J, Abdel-Rasoul M, Kaur B, Fernandez SA, Chiocca EA, Lawler SE (2011) Indirubins decrease glioma invasion by blocking migratory phenotypes in both the tumor and stromal endothelial cell compartments. Cancer Res 71:5374–5380.
Yegutkin GG, Marttila-Ichihara F, Karikoski M, Niemelä J, Laurila JP, Elima K, Jalkanen S, Salmi M (2011) Altered purinergic signaling in CD73-deficient mice inhibits tumor progression. Eur J Immunol 41:1231–1241.
Yin J, Xu K, Zhang J, Kumar A, Yu FS (2007) Wound-induced ATP release and EGF receptor activation in epithelial cells. J Cell Sci 120:815–825.
Zhang B (2012) CD73 promotes tumor growth and metastasis. Oncoimmunology 1:67–70.
Zhang X, Dong XH, Ma Y, Li LF, Wu H, Zhou M, Gu YH, Li GZ, Wang DS, Zhang XF, Mou J, Qi JP (2014) Reduction of a-dystroglycan expression is correlated with poor prognosis in glioma. Tumour Biol 35:11621-11629.
Zhi X, Chen S, Zhou P, Shao Z, Wang L, Ou Z, Yin L (2007) RNA interference of ecto-5′-nucleotidase (CD73) inhibits human breast cancer cell growth and invasion. Clin Exp Metastasis 24:439–448.